ELECTRIC-FIELD-ASSISTED SWIRL-FLAME SYNTHESIS OF HIGH-POROSITY NANOSTRUCTURED TITANIA (TiO_2) FILMS

By

ADITI KULKARNI

A thesis submitted to the

Graduate School-New Brunswick

Rutgers, The State University of New Jersey

in partial fulfillment of the requirements

for the degree of

Master of Science

Graduate Program in Mechanical and Aerospace Engineering

written under the direction of

Professor Stephen D. Tse

and approved by

_____

_____

_____

New Brunswick, New Jersey

January 2015

ABSTRACT OF THE THESIS

ELECTRIC-FIELD-ASSISTED SWIRL-FLAME SYNTHESIS OF HIGH-POROSITY NANOSTRUCTURED TITANIA (TiO_2) FILMS

By ADITI KULKARNI

Thesis Director:
Professor Stephen D. Tse

Nanostructured mesoporous metal-oxide films can be used in various applications, including dye-sensitized solar cells based on titania. Optimization of the properties of these films is crucial in improving their efficiency. Nanostructured TiO_2 films with high uniformity and porosity are grown in a stagnation swirl flame setup under an applied electric field. The effects of external electric-field magnitude and polarity are studied for different substrate temperatures and precursor loading concentrations. The results show considerable differences in film characteristics, for differing electric fields, with more columnar structures and higher porosities under low voltages up to ±400 V. The films have higher packing density at higher voltages of ±800 V. At low substrate temperatures, the morphology and structure are more prominent owing to less on-substrate sintering of the nanoparticles. At low voltages, oppositely-charged particles will be attracted to the substrate increasing the electrophoretic velocity but decreasing the in-flame agglomeration; while at high voltages, the particles will be repelled and stay in the flame longer, thus increasing the in-flame agglomeration. A simple model is proposed which

predicts the trend for deposition of particles and formation of nanostructured TiO_2 films of a given morphology by balancing the effects of thermophoresis, electrophoresis, and Brownian motion of the particles. The model's trend for packing density agrees with the experiments.

ACKNOWLEDGEMENTS

I would like to thank my advisor, Professor Stephen D. Tse for all support and guidance throughout the project. This project would not have been successful without his help. His constant assistance and enthusiasm kept me going whenever I was faced with an obstacle. He was always there to solve any of my problems and answer my queries. I am also grateful to Professor Pelegri and Professor Mazzeo for taking time out of their schedules and reviewing my thesis and providing me with their advice on the editing. Also, support from NASA Grant NNX11AP44A is acknowledged.

All my lab mates have been a great help and tremendous support throughout my work. I would like to thank Dr. Gang Xiong for helping me whenever I had any problems or queries, giving me a hand with the experimental work, sharing his valuable insight on the project and working with me when I had to do any repairs on the setup. He helped me figure out the theories on the project. His guidance was very valuable to me. I would also heartily like to thank Dr. Zhizhong Dong for helping me with the SEM, TEM and XRD. I am grateful to him for taking time out of his schedule every week to help me with the analyzing the samples. He was there to solve any doubts I had with the project or writing the thesis and was always encouraging me during the entire time. I would like to thank Billy Mozet for helping me out whenever I required any assistance in the lab, helping me to find anything and keeping the lab organized. I also thank Hua Hong, Hadi Halim, Ahmed Kamal, Bob Harvath, Michelle Lee and all the members of our group. All of them made my time in the lab a lot of fun and made me look forward to come to the lab.

TABLE OF CONTENTS

LIST OF TABLES

LIST OF FIGURES

CHAPTER 1

INTRODUCTION, LITERATURE REVIEW AND THESIS OVERVIEW

1.1 TiO_2 Nanoparticles and Their Applications

Titanium oxide, such as titanium dioxide or titania is a naturally occurring oxide of titanium. The chemical formula for titanium dioxide is TiO_2. Titanium is found in large quantities in the earth's crust and is the ninth most abundant element[1]. It is found to have a great affinity towards oxygen, and hence it is mostly found in the form of oxides[1]. TiO_2 is a white powder that is odorless and nonflammable. It has a melting point of 1843^oC and boiling point of 2973^oC[1]. It is insoluble in water and has a relative density of 4.26 g/cm^3 at 25^oC.The material properties of titania are influenced by their crystal structure, morphology, and particle size[2,3,4]. In nature, titanium dioxide can be found in three crystalline phases- anatase, rutile and brookite[4,5]. Rutile is the most commonly occurring form of titanium oxide. Anatase and brookite are metastable phases of TiO_2 and irreversibly convert to rutile upon heating above temperatures of 600-800^oC at atmospheric pressure[5–7]. Anatase and rutile have a tetragonal crystal structure while brookite is orthorhombic[5]. The tetragon in anatase crystal has a dipyramidal habit while rutile tetragon has a prismatic habit[8]. Anatase is more chemically reactive than rutile[1,9,10]. It is found to have a lower surface energy than rutile and brookite[4,11–14]. Using the surface energy factor, anatase changes to rutile beyond the particle size of 30 nm[4,11,13]. Also, the solution based chemical methods of preparation of TiO_2 usually form the anatase

structure[4,15–20].

Titanium oxide nanoparticles are vastly used in a variety of applications owing to their high refractive index, photocatalyst properties, aversion to water, opacity, and non-flammability. TiO_2 nanoparticles are used in paints, pigments, dyes, and coatings owing to their light dispersal and chemical stability in sunlight[1,5]. It offers whiteness due to its color for paints and coatings. It also offers opacity and thickness to paints, pigments, and dyes. The consistency of the paints and pigments can be changed by controlling the amount of TiO_2 nanoparticles while manufacturing them. It is also used in the food industry in various foods and food products, medicines, and pharmaceuticals[1,21]. It is used in toothpastes and skimmed milk to give whiteness to them[1]. TiO_2 nanoparticles are largely used in sunscreens because of their high refractive index and strong UV light filtering properties[1,5,22,23].

Anatase TiO_2 is a photocatalyst under UV light. When titanium oxide particles are doped with some metal ions, they may act as a photocatalyst even under visible light and increase the photocatalytic efficiency[6,24,25]. The photocatalytic properties of TiO_2 were first discovered in 1972 by Akira Fujishima[26]. The discovery of this property further led to advances in the use of titanium oxide nanoparticles. It is used in photovoltaics and semiconductors. It has found use in self-cleaning and anti-fogging applications[1]. Titanium oxide nanoparticles are used in the detoxification and purification of industrial waste water[27]. Fujishima[26,28] found that water can be split into hydrogen and oxygen in the presence of titanium oxide as a catalyst under UV light without the application of any

external voltage[29]. This discovery was of extreme importance as it focused in using the hydrogen produced during the water splitting as a clean fuel source.

One of the most important of these applications of titanium oxide with the maximum future scope is in solar cells. TiO_2 has become crucial in the application of dye-sensitized solar cells. Nanostructured mesoporous TiO_2 films are used in dye-sensitized solar cells where they are coated with a thin layer of charge transfer dye[30]. Grätzel[30] studied that excitation of the dye layer in top of the titanium oxide film results in the injection of electrons in the conduction band of TiO_2. These electrons travel through the film and electrolyte to the other electrode and electricity is generated. It has been shown that the efficiency of the solar cell depends on the diffusion of the electrons in the TiO_2 films, which in turn depends largely on the properties of the TiO_2 films, like porosity, particle size, specific surface area, film thickness particle-size distribution, and morphology[31–33]. Efforts have been made to optimize these properties of the mesoporous TiO_2 films to improve the efficiency of the DSSCs[30,33].

1.2 Methods of TiO_2 Nanoparticles and Nanoparticle Films Production

There are various methods being used and developed to produce TiO_2 nanoparticles and TiO_2 nanoparticle films. It is clear from the research on these various methods that different methods will produce nanoparticles of different phases, morphology, structure, and particle size. For example, sol-gel methods are chemical methods to make titanium

oxide nanoparticles and thin films. Efforts are made to optimize these methods to make the nanoparticles more efficient for their use in the applications mentioned above.

The titanium oxide nanoparticles in mesoporous films made from a two-step sol-gel method were found to have small particle size distribution, minor surface defects, and high crystallinity[34]. The nanoparticle films produced by this method were used in dye sensitized solar cells, and their performance was measured to investigate the photovoltaic efficiency. TiO_2 nanoparticles of anatase phase of uniform size were made by a sol-gel process from a condensed $Ti(OH)_4$ gel[35]. It was found that the size of the particles changed with an increase or decrease in the pH of the $Ti(OH)_4$ gel. Ti-triethanolamine also controlled the shape of the anatase TiO_2 nanoparticles. Thin films were made from titanium oxide nanoparticle colloids formed by sol-gel method[36]. The nanoparticle colloids were grown in a hydrothermal atmosphere with controlled conditions. The thin films were found to have rod like structure of the particles with long axis.

Another most important method of synthesis of titania nanoparticles is flame synthesis. In this method, a precursor with titanium in it undergoes combustion in a certain type of flame to decompose and form TiO_2 nanoparticles. It has been found that the size, structure, and other characteristics of the nanoparticles can be controlled efficiently with the flame synthesis methods. Some of these methods are discussed below.

A premixed laminar flat flame aerosol reactor was used to synthesize TiO_2 nanoparticles using $TiCl_4$ as a precursor[37]. The average size of the nanoparticles formed was 13 nm.

The mesoporous films used for DSSCs were formed by a flame stabilized by a rotating surface which was used as a substrate for the nanoparticle deposition by Nikraz et. al[33].. The rotating substrate ensured that the deposition of the nanoparticles on the film is uniform with constant thickness. The performance of the mesoporous films in the DSSCs was measured to find the efficiency of the solar cells. Kavitha et. al[38] studied the effect of substrate temperature, precursor concentration and synthesis time on the properties and phase of TiO_2 nanoparticles synthesized in a flame pyrolysis reactor. A silicon substrate was used for deposition of the titanium oxide films. They found a change in the phase of the nanoparticles with a change in substrate temperature. A flame aerosol reactor was used to produce titanium oxide nanoparticle films by Thimsen and Biswas[39]. They studied the effect of precursor concentration and substrate temperature on the nanostructured TiO_2 film properties. The influence of operating pressure and precursor concentration on the properties of TiO_2 nanoparticles synthesized in a low pressure H_2-N_2-O_2 burner stabilized premixed stagnation flat flame was studied by Zhao et. al[40]. Titanium tetra-isopropoxide (TTIP) was used as precursor for the synthesis.

A new type of premixed-stagnation swirl flame was introduced by Wang et. al[41] for the synthesis of titanium dioxide nanoparticles. The setup has a swirl chamber introduced inside the burner which gives turbulence to the flame. The mean diameter of the particles synthesized by this method was 5-10 nm. Zhang et. al[42] used premixed stagnation swirl flame synthesis setup to grow highly-porous nanostructured TiO_2 films. The different properties and characteristics of the titanium oxide nanoparticle films, like size, morphology, and structure of the films, were controlled by changing the substrate

temperature and precursor concentration. Interesting changes in the average size of the particles and the structure and growth of the films were found when the substrate temperature was changed or when the precursor concentration was varied. The growth and structure of the films was controlled by the competition between Brownian motion and thermophoretic velocity acting on the particles incident on the film.

Apart from these methods of synthesis, other methods such as microemulsion, hydrolysis, and thermohydrolysis are also used for synthesis of titanium oxide nanoparticles[43].

1.3 Effect of Electric Field on the Growth of Titanium Oxide Nanoparticles

Research has been conducted to study the effect of an externally applied electric field on the titanium oxide nanoparticle size, morphology, structure, and other properties. Kammler et. al[44] studied the formation of TiO_2 nanoparticles synthesized in a CH_4-O_2 pre-mixed flame. They applied a DC electric field with the help of plate electrodes and studied its effect on the temperature of the flame. The effects of this electric field on the particle size, crystallinity, and morphology were studied with the help of Fourier transform infrared spectroscopy. The particle size was found to decrease under the electric field. The effects of external applied electric field on TiO_2 nanoparticles were also studied by Katzer et. al[45] in a CH_4-O_2 premixed flame reactor. The changes in particles size, morphology and flame temperature were studied for three types of electrode pairs namely needle, plate and sphere. For example, the needle electrodes

increased the agglomerate size of the particles while plate electrodes decreased it. The primary particle size and rutile content were found to change due to the applied electric field. The properties and growth of titanium oxide nanoparticles under uniform electric fields synthesized in a low-pressure premixed stagnation flame was studied by Zhao et. al[46]. The effect of electrophoretic velocity due to the applied electric field was studied on the growth and transport of particles. The experimental results showed different particle sizes under different electric field strengths and proved that electric field application can decrease the average particle aggregate size.

1.4 Overview of the Thesis

As seen from the research of the effects of applied electric field on the synthesis of titanium oxide nanoparticles, there is an obvious change in the properties of the titania nanoparticles, especially the particle size, under the electric field as opposed to those grown without the application of any electric field. Also, the methods of synthesis to grow TiO_2 nanostructured films with a high porosity are researched, as highly porous films will increase the efficiency of the DSSCs.

In this the thesis, the two are combined such that TiO_2 nanostructured films are grown in an electrically-assisted premixed stagnation swirl-flame synthesis setup on a silicon substrate. The external high voltage is applied to the substrate (with the burner grounded) to study the effects of the external electric field on the growth, structure, size, morphology, porosity, and crystallinity of the TiO_2 films. The effect of different electric

field strengths and the polarities of the field on the titanium oxide films are also studied. A negative voltage applied to the substrate will cause a negative electric field in the flame while a positive voltage applied to the substrate will result in a positive electric field in the flame. The substrate temperature and precursor concentration are varied to study how the combination of changing electric field strengths, substrate temperature, and precursor concentration affects the growth and structure of the titanium oxide films. Ex-situ characterization is performed on the films to find the size of the nanoparticles, the thickness and structure of the films, and the phase of the particles, as well as the porosity of the films. The thesis explains in detail the experimental setup; procedures of conducting the experiments; results and discussion; and conclusions and future scope.

CHAPTER 2

EXPERIMENTAL SETUP AND PROCEDURE

2.1 Experimental Setup and Configuration

The main components in the setup for the experiment to study the effects of an electric field on the nanostructured titanium oxide films produced by swirl flame synthesis are the swirl flame burner; the substrate; the high voltage power supply; the gasflow delivery system with mass flow controllers and the heaters; the precursor flow and heating setup; and the temperature probes. The burner and the substrate with the cooling water supply configuration are enclosed in a hood with an exhaust. The burner, substrate, and gas and precursor flow controllers are arranged on a 5x3 feet base mounted on a table of 3 feet height with wheels for ease of moving the entire setup.

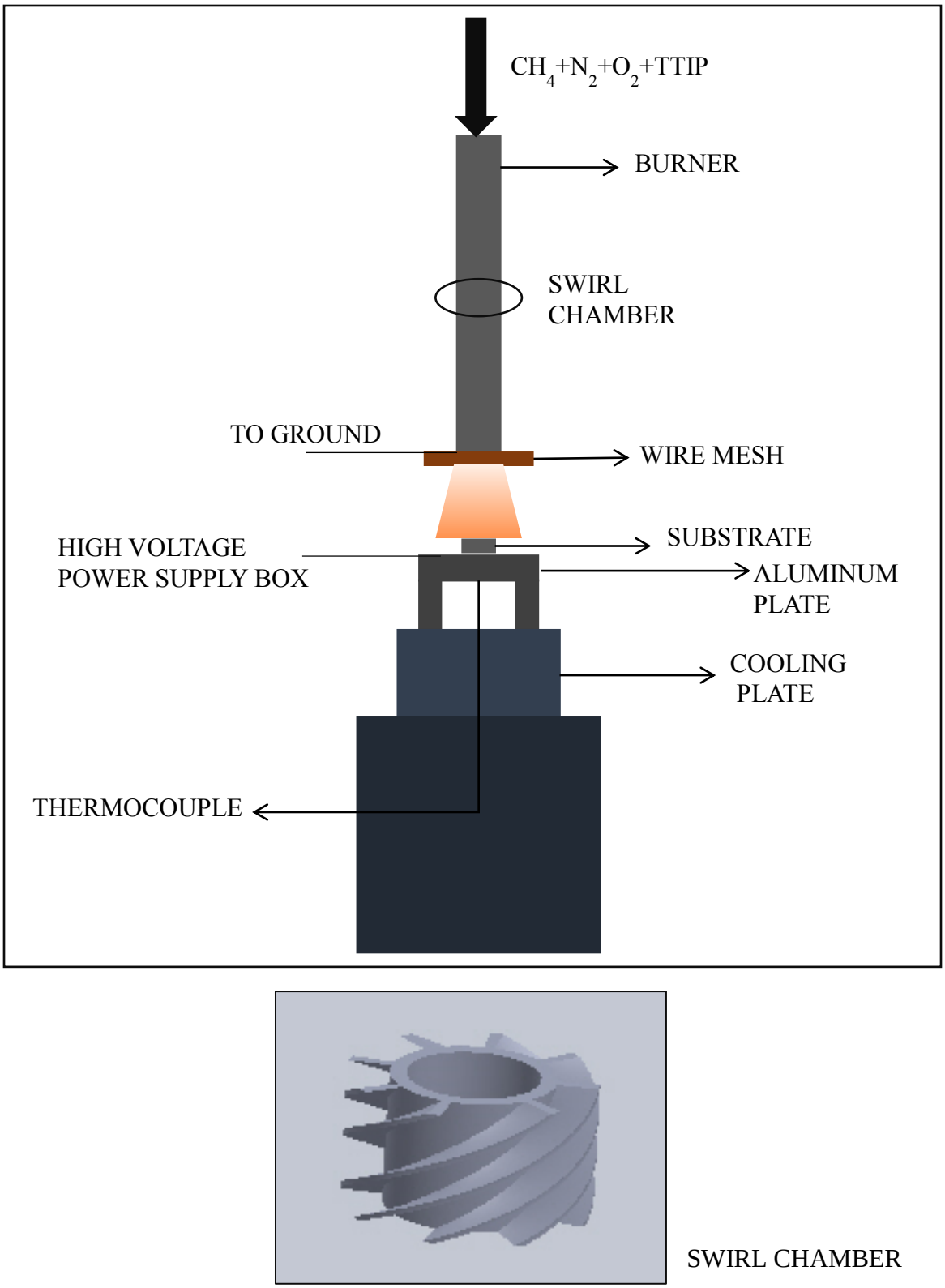

Figure 2.1. Experimental Setup of the Swirl Flame Burner.

2.1.1 Swirl Flame Burner

The swirl flame burner is a stainless steel cylindrical tube with a swirler. The tube has an internal diameter of 18mm and a length of 200mm with threads at the top to fix it into a top plate which holds the burner in a vertical position. The swirler is located inside the burner at a distance of 70mm from the tube exit. The swirler has an outer diameter of 18mm and is 14mm in length. The swirler consists of annular vanes at the circumference with a tubular bypass at the center with an outer diameter of 8mm. The top of the tubular bypass is fitted with a perforated screen. The swirler has eight blades at an angle of 45^{o}. The swirl number is dependent on the ratio of the jet of gases flowing through the central bypass to the gases flowing through the swirl vanes. This swirl number can be varied by changing the mesh density on the perforated screen. The swirl number for this experiment is set at 0.248, producing low-swirl flame [41].

2.1.2 Substrate

A silicon wafer 380µm in thickness is used as a substrate on which the TiO_2 films are grown. The substrate is a small piece of silicon about 10mm x 10mm obtained by fracturing the silicon wafer using a diamond cutter. The substrate piece is further fractured in two 5mmx10mm parts which are then placed side by side to grow the film. The purpose of using two pieces is to get a cross-section of particle deposition to view the TiO_2 structure under SEM. The silicon substrate is placed on an aluminum plate 12cm x 12cm and 5mm thickness. A very thin layer of thermal grease is applied between the two

to increase the thermal conductivity. The grease is electrically conductive so that the electric field applied to the aluminum plate flowing to the silicon substrate is not affected. A cooling plate is placed below the aluminum plate separated by quartz blocks with thermal grease applied between the layers. The thermal grease from Omega Engineering used here is electrically insulating as we want the aluminum plate to be completely isolated. The distance between the aluminum plate and cooling plate can be changed by adding or decreasing the quartz blocks[42]. The cooling plate has cooling water circulating through it whose flow can be controlled by a valve. The temperature of the aluminum plate can be changed by adjusting the water flow through the cooling plate and the distance between the two plates. A K-type thermocouple is placed between the cooling plate and the aluminum plate which measures and displays the temperature at the base of the aluminum plate. The temperature of the silicon substrate can be calculated using conduction heat transfer calculations where the thickness and thermal conductivity of the aluminum plate, thermal grease, and silicon substrate are known. The whole substrate setup is mounted on a truss platform.

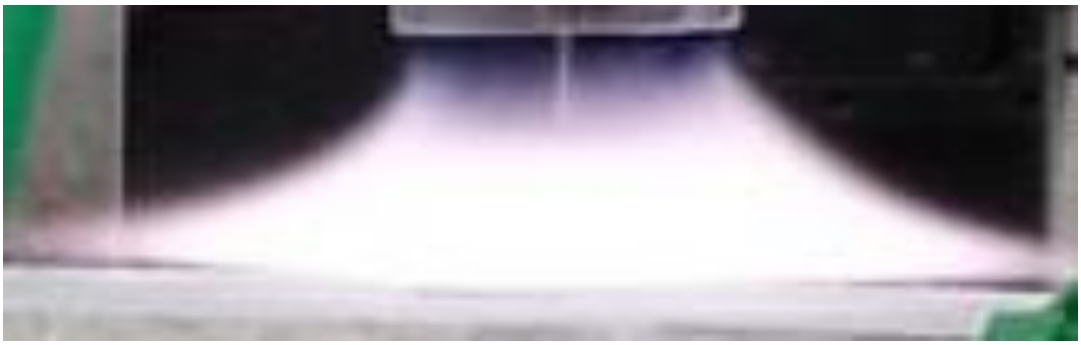

Figure 2.2. Stagnation swirl flame.

2.1.3 Gas Flow Controllers

The gases used for the experiment are:

High Purity Nitrogen- NI HP 300, purity>99.998%,

Industrial Oxygen- OX 300, and

Industrial Methane- chemically pure, purity>99.5%.

The gases are metered to the setup using mass flow controllers. The mass flow controllers have a maximum flow rate of fluids which can pass through them. A digital command module from AALBORG is used in the setup. It generates a 0-5V signal which is directly proportional to the flow rate of gases through the controllers. A percent value for the gases can be entered in the command module which will allow that percent of gas from the total flow rate of the mass flow controller to pass through it. The gases are setup at the given percent of the total flow rates of the mass flow controllers:

N_2- 90%

O_2- 35%

CH_4- 29.1%

The resultant flow rates of the gases are

N_2- 2.25 L/min

O_2- 6.60 L/min

CH_4- 24.9 L/min

Figure 2.3. AALBORG Command Module.

2.1.4 Precursor Setup

Titanium tetraisopropoxide (TTIP) from Sigma Aldrich with 97% purity is the precursor used for this experiment. The precursor is kept in a glass bubbler which is radiantly heated up to 80^{o}C. The carrier gas used for the TTIP line is nitrogen which will be discussed in the next section.

2.1.5 Gas and Precursor Lines

A mixture of N_2+O_2+CH_4 with the above mentioned flow rates is mixed and passed through a gas line and heated up to 120^oC with a rope heater. A thermocouple (K-type) is used to measure the temperature of the gas line. A bypass line with N_2 as the carrier gas for TTIP merges with the precursor line downstream of the bubbler. The precursor line is heated up to 130^oC with a rope heater, measured by a thermocouple, to avoid condensation of the precursor in the line. N_2 is the carrier gas used for TTIP in the precursor line. Further down the flow, the precursor and the premixed gas mixture of oxygen, nitrogen and methane are mixed in a line prior to the burner and heated up to 120^oC with a rope heater. A temperature controller is used to maintain the temperature. The temperature of the mixture is measured just before the entry to the burner with a thermocouple. The temperature at this point should reach 76.6^oC before starting the flame. Table 2.1 shows the gases passing through the respective gas lines and the temperatures to which they are heated using a rope heater. It also shows the thermocouples attached to the respective gas lines.

Gas Line	Gases	Thermocouple	Temperature
A	CH_4+O_2+N_2	A	170^oC
B	TTIP	B	130^oC
C	TTIP+ CH_4+O_2+N_2	C	120^oC
E	before the burner	E	170^oF

Table 2.1. Flow of gases through the gas pipes and the temperature to which they are heated.

2.1.6 High Voltage Power Supply

A high voltage power supply box, GenCom Division High Voltage Power Supply Box, -/+ 0-3 kV is used to supply electric field to the setup. The high voltage line is connected to the aluminum plate while another line is connected from the burner to the ground connection on the box. The ground line from the box and the lines from the setup table are connected to the main ground point in the lab. Thus, all the setup including the box is appropriately grounded. The aluminum plate is isolated from the cooling plate using quartz blocks and electrically insulating thermal grease to ensure that the electric field does not leak from the aluminum plate to the cooling plate or the setup table. The power supply box has a switch to change the polarity and a dial which adjusts the voltage strength being applied.

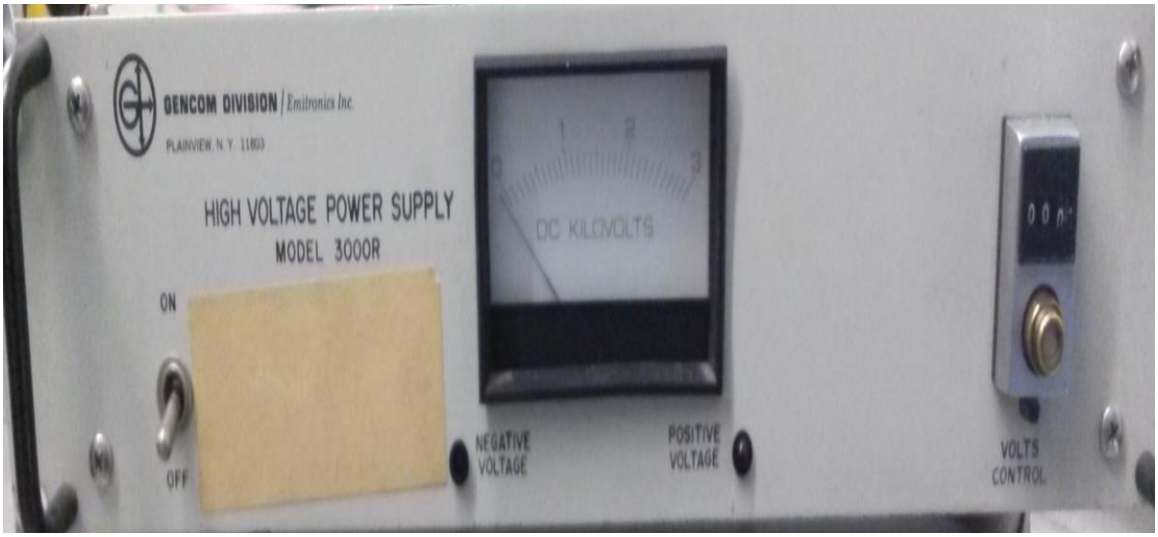

Figure 2.4. High Voltage Power Supply Box.

2.2 Experimental Procedure

This work focuses on the effects of an electric field on the TiO_2 nanoparticles film structure, porosity, and morphology. A set of 9 experiments is run for a fixed substrate temperature and precursor concentration by varying the voltage from -800 V to +800 V with an interval of 200 V. Table 2.2 below shows all the cases runs, with the synthesis time for each. Adjusting the nitrogen carrier gas flow rate can change the precursor concentration and the substrate temperature can be adjusted by changing the thickness of the quartz blocks and the cooling water flow rate. The accuracy of the substrate temperature measured by the thermocouple is ± 10^oC. In the first part, the substrate temperature is changed (473 K, 663 K and 763 K) while the precursor concentration is kept constant at 116 ppm; and the experiments are run for each case by varying the electric field. In the second part, the precursor concentration is changed (29.1 ppm, 116 ppm, 232.8 ppm and 291 ppm), while the substrate temperature is kept constant at 763 K and similar experiments are performed[42]. As the precursor concentration is changed, the synthesis duration is varied accordingly in order to keep the total amount of precursor added in each case to be the same[42]. Table 2.2 shows all the cases run with the parameters of substrate temperature, precursor concentration, and synthesis duration.

CASE	SUBSTRATE TEMPERATURE (K)	PRECURSOR CONCENTRA-TION (ppm)	SYNTHES-IS DURATION (s)	FILM CHARACTER-IZATION	VOLTAGE APPLIED
1	473	116	300	SEM, TEM, XRD, Packing Density	-800V to 800 V
2	663	116	300	SEM, Packing Density	-800V to 800 V
3	763	116	300	SEM, Packing Density, TEM	-800V to 800 V
4	763	29.1	1200	SEM, Packing Density	-800V to 800 V
5	763	232.8	150	SEM, Packing Density	-800V to 800 V
6	763	291	120	SEM, Packing Density	-800V to 800 V

Table 2.2. All cases of experiments run.

The steps to carry out an experiment are:

1. Adjust the thickness of the quartz blocks and apply a thin layer of thermal grease between each layer to get the required temperature of the substrate in the flame.

2. Prepare the silicon substrate and place it on the aluminum plate by applying a small amount of thermal grease.

3. Start the cooling water flow.

4. Turn on the rope heaters for the gas lines.

5. Start the flow of compressed air through the gas lines which is used for preheating the setup.

6. Adjust the digital controller and make sure the flow rates of the gases are set to the values mentioned above.

7. Adjust the N_2 carrier gas flow rate to get the required TTIP concentration.

8. Enter the temperatures for the controller that the gas lines need to be heated to.

9. Make sure there is enough TTIP in the bubbler and enough gas in the cylinder tanks.

10. If the TTIP in the bubbler is not enough, fill it up.

11. Start the heating of the TTIP in the bubbler.

12. Let the setup preheat for about 20 minutes until the temperature of the gases just before the burner reaches about 170-180^{o}F as seen from Thermocouple E.

13. Make sure the connection of the high voltage line from the power supply box to the substrate is secure.

14. Make sure all the connections are grounded.

15. Place the hood on the burner.

16. Once the setup is warmed up to the required temperature, turn off the compressed gas supply and open the nitrogen valve to start the nitrogen flow through the lines.

17. Make sure the nitrogen flow rate is constant and start the oxygen flow rate.

18. Make sure the oxygen flow rate and the temperatures are constant; and open the methane valve.

19. Ignite the flame just below the burner when the methane flow rate is constant.

20. Observe the flame to when you get a “steady” flame.

21. Turn on the high-voltage power supply box (**For the case of no electric field, skip to step 24**).

22. Set the polarity by flipping the switch for negative or positive voltage.

23. Turn the knob to adjust the voltage to the required magnitude.

24. Open the precursor valve to start the TTIP flow.

25. Slowly close the valve on the bypass line and watch the flame carefully. In case of any problems or issues, open the bypass line and close the precursor valve.

26. Once the TTIP is added, start the timer and run the experiment for the required time depending on the case being run.

27. Once the timer stops, open the bypass line and close the precursor line (**For the case of no electric field, skip to step 30**).

28. Adjust the knob on the supply box to zero.

29. Turn off the power supply box.

30. Close the methane valve.

31. Close the oxygen valve.

32. Start the compressed air to flow through the lines.

33. Stop the heating by unplugging the rope heaters.

34. Close all the cylinder tanks.

35. Let the setup cool down, and then turn the compressed air supply off.

36. Collect the TiO_2 films on the silicon substrate carefully and store them in a case, along with proper identification.

CHAPTER 3

EX-SITU CHARACTERIZATIONS

3.1 Field Emission Scanning Electron Microscope (FESEM)

The images of the titanium oxide films are taken using a FESEM. The structure and the growth of the nanoparticles on the film are studied using a magnification from 2000 X up to 30K X. The films are mounted vertically in a copper grove that is mounted on a stud and stuck on using a carbon tape. The samples are inserted vertically inside the FESEM such that the cross-section of the TiO_2 film on the edge of the substrate is visible in the frame, presenting a side view of the film.

3.2 High Resolution Transmission Electron Microscope (HRTEM)

The HRTEM is used to obtain further magnified images of the titania nanofilms, which can be used to find the average primary size of the constituent particles. The sample is prepared by scrubbing off a small amount of titania powder from the film surface and sonicating it in ethyl alcohol. A couple drops of the mixture are then poured on the carbon grid using a pipette. The grids are then inserted in the TEM. The size of the particles can be found by using the software to view and measure TEM images - the Digital Micrograph. The composition of the nanoparticles is found by Selected Area Electron Diffraction (SAED).

3.3 X-Ray Diffraction (XRD)

The composition of the TiO_2 nanoparticles is also found using XRD analysis. The nanoparticles taken from the substrate after the experiment are placed inside a small circular indentation in a disc and a drop of ethyl alcohol is added to get a thin layer of the powder. The sample is then inserted in the XRD and the analysis is run for 15 minutes. The XRD analysis gives the composition of the particles as well as the average diameter of the particles in the sample.

CHAPTER 4

PACKING DENSITY

4.1 Introduction

Packing density of a film is the property used to assess how the particles are packed together. It is used to find the porosity of the film. As mentioned above, a higher porosity film is desired to obtain a greater efficiency from the dye-sensitized solar cells. The porosity of the particle films can be found from the packing density as (1- packing density)*100 which will be in a percentage form. The packing density of the films can be found from the experiments performed. In addition, a deposition model is prepared to simulate the deposition of the particles in the flame on the film and the packing density can be estimated from this.

4.2 Methods to Calculate Packing Density

4.2.1 Experimental

The packing density of a TiO_2 film grown under the SSF can be determined from the experiments. The formula used to calculate the packing density is:

$$\boldsymbol{\varepsilon = \frac{m_f}{\rho A_f h_f}} \quad (1)$$

Where, ε is the packing density, m_f is the weight of the film measured by the weighing scale Mettler AE 240 (accuracy $10^{(-5)}$ grams), ρ is the density of TiO_2 (3840 kg/m^3), A_f is the area of the film, and h_f is the thickness of the film found from the SEM images of the cross-section of the films. The weight of the film is found by measuring the substrate along with the film, then scraping off the film just to weigh the substrate. The difference between the two is the weight of the film. The area of the film is calculated by measuring the length and width of the substrate.

4.2.2 Correlation-The Deposition Model for Packing Density

In order to explain the value of the packing density of the TiO_2 films, we constructed a simple deposition model similar to Zhang et. al[42]. The deposition of the particles is affected by the surface forces and particle inertia due to which an incident nanoparticle sticks to one already deposited on the film, thus obstructing its further penetration into the film. The two main processes in the flame which govern this deposition of the particles are - the thermophoretic velocity caused by the temperature gradient between the burner and the substrate (which controls the penetration depth of the incident particle in the film) and the Brownian motion caused by the colliding molecules (which affects the probability of the incident particle to attach to a deposited one). A set of equations were used to calculate the mean penetrating time (τ_p), thermophoretic velocity ($v_{th/e}$), and the penetration distance (l_{pene}) of the nanoparticle in the film. The mean penetrating time is calculated using the average Brownian velocity (v_B), the concentration of the primary

particles in the film structure (c_f) and the travel distance of the incident particles prior to deposition in the film (l_p). The following equations are used to calculate these parameters:

The average Brownian velocity[47], $v_B = \left(\frac{3\mathrm{kT}}{\mathrm{m_p}}\right)^{\frac{1}{2}}$ (2)

where, m_p is the mass of the particle, k is the Boltzmann constant, and T is the absolute temperature.

The concentration of the primary particles in the film is given by

$c_f = \frac{\varepsilon \mathrm{f}}{(\mathrm{d_{pf}})\text{^}3}$ (3)

Where, ε is the average packing density, f is the correction factor taken as 0.5, and d_{pf} is the diameter of primary particles in the film.

The 'mean free distance' of the primary particle before deposition in the film (l_p) is the distance travelled by the particles before their "horizontal" collision with the particles already deposited in the porous film and can be modeled by basic collision theory in the free molecular regime,[48,49] as shown below

$l_p = \frac{(\frac{1}{c_f})}{S_e}$ (4)

where, S_e is the cross-sectional area for collision given by

$S_e = \beta\frac{\pi}{4}\left(\mathrm{d_{pi}} + \mathrm{d_{pf}}\right)^2$ (5)

where, β is the enhancement factor for collision rate, d_{pi} is the diameter of incident primary particles in the flame, and d_{pf} is the diameter of primary particles in the film.

Thus, the mean penetrating time, i.e. the time taken by the primary particle inside the flame to collide "horizontally" with particles in the film where it is captured and deposited, is expressed as

$$\tau_p = \frac{l_p}{v_B} \tag{6}$$

Both l_p and τ_p are dependent on the Brownian motion of the particles in the flame and their probability to collide in a horizontal direction with the particles deposited in the flame.

The particle movement in the perpendicular direction (with respect to the substrate) depends on the total effect of thermophoresis, electrophoresis, gravitational force, and drag force acting on the particle. An expression for particle velocity is formulated from the combination of the thermophoretic force (F_{th})[50,51], electrophoretic force (F_e)[51], gravitational force (F_g)[51] and equating it to the drag force (F_d)[51] by Stoke's law as given below

$F_{th} + F_e + F_g = F_d$

$$\frac{(3\pi\eta_{gas}^2 r\times\nabla T)}{\rho_{gas} T1} + \frac{(qV)}{D} + \frac{(4\pi\times r^3\rho_p g)}{3} = \left(6\pi\mu_{gas} r v\right) \tag{7}$$

where, η_{gas} and ρ_{gas} are the viscosity and density of gas respectively, ∇T is the temperature difference between the burner exit and the substrate, q is the unit charge on

the particles, *V* is the voltage applied to the substrate, *D* is the distance between the substrate and burner exit, T_1 is the temperature of the flame at the burner, *r* is the radius of the primary particle in the flame, g is the acceleration due to gravity, μ_{gas} is the dynamic viscosity of the gas and *v* is the relative velocity of the particle. We can find absolute velocity of the particle v_p from *v* using the equation below and substitute it in equation (9).

$$v = v_p - v_{gas} \tag{8}$$

where, v_{gas} is the velocity of the gases in the flame.

Using the above expressions, the penetration distance for particles is calculated

$$l_{pene} = v_p \times \tau_p \tag{9}$$

The packing density is assumed to be proportional to the penetration distance. A proportionality factor "*x*" is used such that the penetration distance is *x* times the packing density. A case at 116ppm and substrate temperature 763K is used as a reference point to determine this factor "*x*" or the constant of proportionality. This factor remains constant for all the other cases and the penetration distance is found using this factor in equations from 3-8. Using an iterative method, the packing density is found for all the cases[42].

CHAPTER 5

EFFECTS OF ELECTRIC FIELD AND SUBSTRATE TEMPERATURE

5.1 Introduction

In this chapter, we will study the first three cases shown in table 2.2. In these cases, the precursor concentration is kept constant at 116 ppm and the substrate temperature is changed for every case. The temperature of the substrate for the 1st case is set at 473 K, for the 2nd case at 663 K, and for the 3rd case at 763 K. The temperature is held throughout the experiments for each case with an accuracy of ±10^{o}C. The temperature of the substrate is adjusted by changing the distance between the aluminum plate and the cooling plate by increasing or decreasing the thickness of the quartz blocks and by adjusting the flow rate of the cooling water. For the low substrate temperature of 473 K for case 1, the thickness of the quartz blocks is a very thin layer of about 2-3mm and the flow rate of cooling water is maximum. For the case 2 with 663 K as substrate temperature, the thickness of the quartz blocks is increased up to 4-5mm and the flow rate of cooling water is almost halved. For case 3 with 763 K, the thickness of the quartz blocks is about 5-6 mm; and the flow rate of cooling water is minimum with the water valve just barely open. The temperatures of the substrate for the respective cases are confirmed by starting the flame without adding the precursor and measuring the substrate temperature using a pyrometer. As all the cases have the same precursor concentration, they run for the same time of 300 seconds. Each case has 9 sets of experiments:

1. No electric field applied or 0 V

2. -200 V
3. -400 V
4. -600 V
5. -800 V
6. 200 V
7. 400 V
8. 600 V
9. 800 V

Below, each case is discussed for the above experiments and their results.

5.2 CASE 1:
Precursor concentration – 116 ppm
Substrate temperature – 473 K
Synthesis time – 300 seconds

5.2.1 Introduction

Case 1 has the concentration of N_2 carrier gas set at 45% in the digital command module, and the TTIP is heated up to 80^{o}C to achieve a TTIP concentration of 116 ppm introduced to the flame. The substrate temperature is set at 473 K and confirmed using a pyrometer. The substrate temperature during experiments can be observed from the display of the K-type thermocouple. The temperature remains constant with an accuracy of ±10^{o}C. 9 experiments of 300 seconds each are run by varying the applied voltage to

the substrate from -800 V to +800 V, as given above. The results for the experiments are shown below in the next section.

5.2.2 Results

5.2.2.1 SEM

Figure 5.1 shows the SEM images of cross-sections of the nanostructured TiO_2 films. Image for 0V shows the film when there is no voltage applied to the substrate. In the absence of any electric field, the structural growth of the film is similar to the one shown by Zhang et.al[42] for the same substrate temperature and precursor concentration. The SEM images show a more columnar growth at low voltages till |±400 V|, which is consistent with the simulations of deposition of particles in an electric field by Kulkarni and Biswas[52]. The film synthesized under a negative electric field seems more porous with smaller primary particle size, while the film synthesized under a positive electric field looks more packed with a higher aggregate size. For a low substrate temperature, the thermophoretic velocity and Brownian motion dominate the deposition of particles on the film. This results in the tree-like branched structure of the TiO_2 film similar to those shown by Thimsen and Biswas[39], as well as Thimsen et.al[53]. In addition to these regimes, with the application of electric field, the electrophoretic velocity will also play role in structuring the film[52]. The columnar growth of the TiO_2 nanostructured film under an electric field can be explained by combining the effects of electrophoresis and thermophoresis, which will cause the film to grow in a vertical direction. Further

discussion on the structure and porosity of the films is done in the later section.

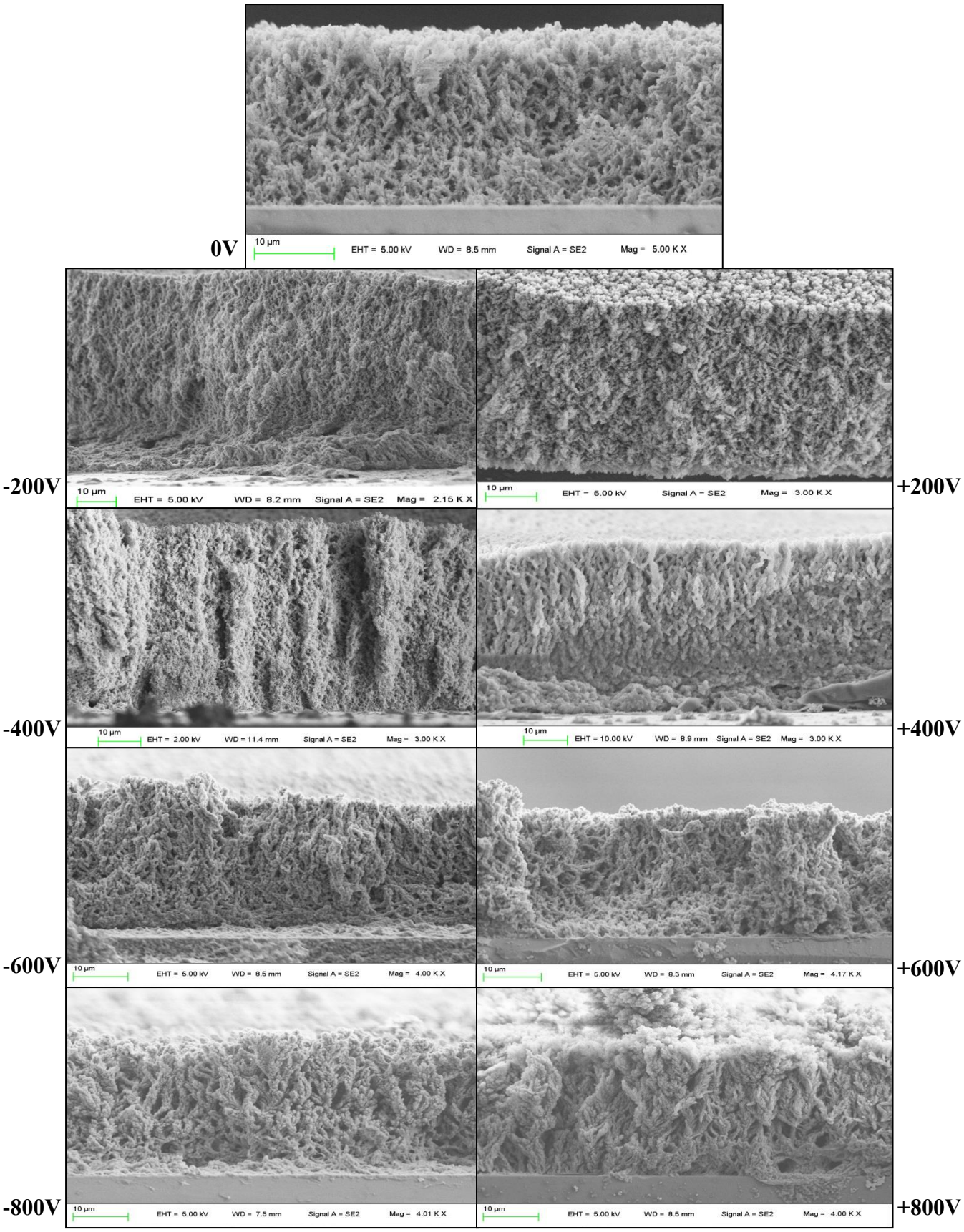

Figure 5.1. SEM images of TiO_2 films for CASE 1.

5.2.2.2 XRD

Figure 5.2 shows XRD analysis of the TiO_2 nanoparticles collected from the surface of the substrate. The analysis shown in the figure is for the case when there is no electric field applied to the substrate. It confirms the phase of the nanoparticles to be anatase. The phase of the particles remains the same irrespective of the electric field applied to the substrate. Thus, the electric fields applied in this work do not affect the phase of the particles produced in the flame.

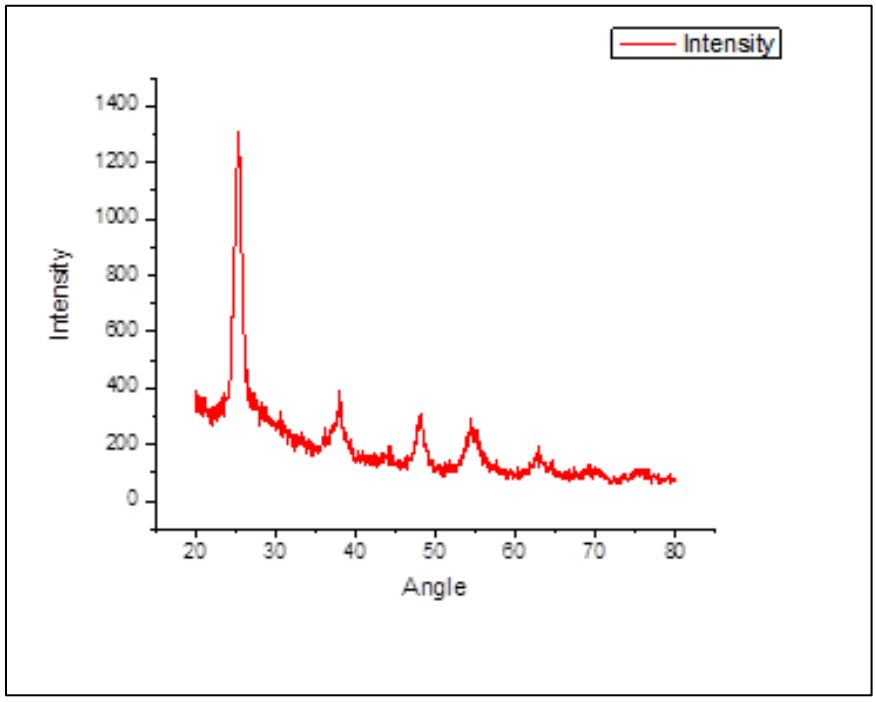

Figure 5.2. XRD analysis of the TiO_2 nanostructured film in the absence of electric field for case 1.

5.2.2.3 TEM

Figure 5.3 below shows the TEM images of titanium oxide nanoparticles taken directly from the TiO_2 films grown on the silicon substrate for the above mentioned substrate temperature and precursor concentration. The three images show particles produced under no electric field, under a voltage of -400 V, and under a voltage of +400 V respectively. The average primary particle size of the particles is found by measuring 20-30 nanoparticles in the TEM using software Digital Micrograph. We can see from image for 0V that ultrafine particles are produced in the stagnation swirl flame (SSF) even in the absence of any external electric field. The average primary particle size in this case is 4-6 nm. Also, as the substrate temperature is low, there is insignificant on-substrate sintering resulting in less particle agglomeration/aggregation[41]. The average primary particle size for the -400 V case is similar to that in the absence of electric field, i.e. about 3-5 nm. However, in the case of +400 V it can be seen that the particles are much larger; and the average primary particle size is about 8-10 nm. Thus, we can conclude that the average particle size of the TiO_2 nanoparticles is much smaller when a negative voltage is applied than when a positive voltage is applied. Due to thermionic emissions, the particles maybe more positively charged. As a result, they are attracted to the low magnitude negative voltage applied on the substrate accelerating the particles in the flame. The resident time of the particles in the flame reduces resulting in smaller particle size. However, the positively charged particles will be repelled from the low magnitude positive voltage on the substrate, increasing their residence times in the flame and in turn the particle size.

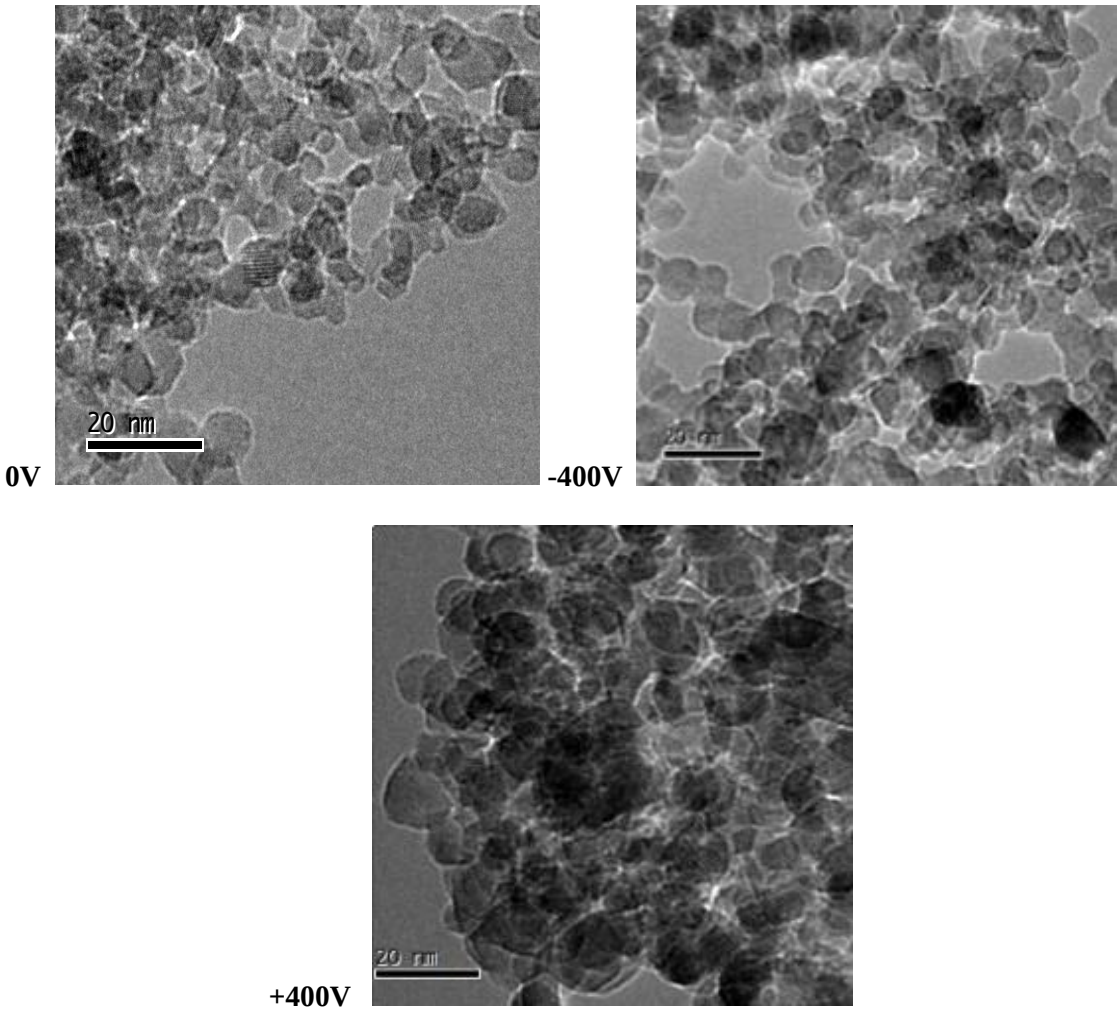

Figure 5.3. TEM images of TiO_2 nanoparticles

5.2.2.4 Packing Density

Figure 5.4 shows the graph of packing density calculated for TiO_2 films formed under all the 9 experiments under voltages ranging from -800 V to +800 V. The graph shows packing density calculated both from the experiments and the correlation model. The method used to obtain the packing density from experiments and the correlation model is explained in the earlier section. Though the values are not exactly the same, the trend in

both cases is similar showing a lower packing density at lower magnitudes of voltages up to |±400 V|, after which it increases. Also, by both experimental and correlation methods, the packing density is seen to be minimum at -400 V. The figure clearly shows that the deposition of the particles and porosity of the film is affected under an electric field and depends on the magnitude of the applied voltage. The possible explanation for such a trend is discussed in the next section.

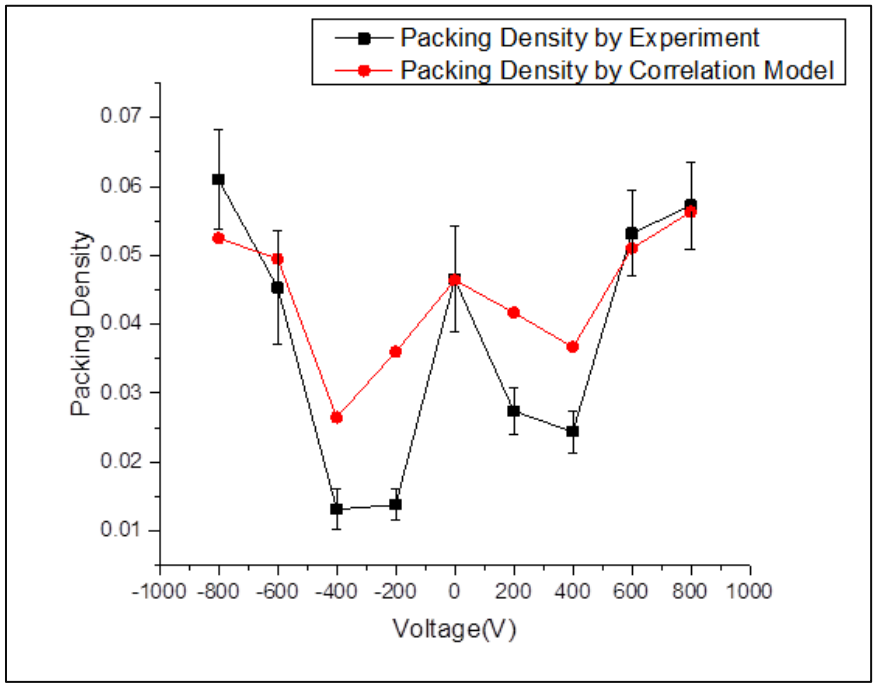

Figure 5.4. Packing Density of the TiO_2 film for case 1 under a voltage from -800 V to +800 V by experiment and model calculations.

5.2.3 Discussion

The effect of the applied electric field on the packing density of the nanostructured titanium oxide films can be explained by the two main regimes that seem to be affecting the particle movement and growth in the film: i) the electrophoretic velocity ii) the average size of the primary particles in the flame incident on the film. The observations of these two regimes can be seen in the experimental ex-situ characterization as well as from the results in the deposition model.

We assume the flame to consist of TiO_2 nanoparticles both positively and negatively charged, but not necessarily in equal distributions, since the "hot" flame can induce thermionic emission. As seen from the trend in Figure 5.4, the packing density of the TiO_2 films is less at lower voltage magnitudes of ±200 V and ±400 V, and increases as the voltage magnitude increases above |± 400 V| (as can be seen at ±600 V, ±800 V). The lowest value of the packing density is at -400 V. This trend can be explained using the TEM images and the deposition model equations. The average particle size calculated from the TEM images shows that the average primary particle diameter is smaller for -400 V than for -800 V. Similarly, it shows that the average primary particle size for +400 V is smaller than for +800 V. These results are similar to the results obtained by Zhao et. al[46] by applying an electric field in a low-pressure premixed flame. Thus, for either polarity, the particle size seems to be increasing with increasing magnitude of the voltage. When the applied voltage is low, the charged particles are attracted to opposite polarity on the film. For example, if it is a negative electric field, the positively charged

particles will be attracted to the film. This attraction will increase the electrophoretic velocity causing the particles to move faster through the flame. Thus, the particle should penetrate deeper and the film should be more packed. However, these particles will spend less time in the flame, being subjected to less in-flame agglomeration and particle growth, resulting smaller primary-particle sizes, as confirmed by the TEM. (A smaller particle will also have larger Brownian velocity, which outweighs the electrophoretic effect). A combination of this electrophoretic velocity in the flame and the resultant particle size will create a loosely packed film, decreasing the packing density as concurred from the equations in the deposition model.

Inversely, when a high voltage is applied to the substrate, it accelerates the particles in the flame inducing stronger molecular collisions with each other to form positive and negative ions. If the polarity of the voltage on the substrate is negative, the positive ions will attract to the substrate. At the same time the electrons will be repelled back into the flow field colliding with molecules producing more positive ions and electrons. These electrons attach to neutral molecules forming negative ions which in turn attach to particles to give them a negative charge. This will increase the negatively charged particles in the flame which will be repelled from the substrate decreasing the electrophoretic velocity. Conversely, when a high magnitude positive voltage is applied to the substrate, the electrons will attract to the substrate while the positive ions will attach to the particles giving them a net positive charge. Thus, the positively charged particles will repel from the substrate back into the flow field. Although one may expect this effect to result in a loosely packed film, the particles will spend a longer time in the

flame, where in-flame agglomeration and particle growth will cause the average primary particle size to increase. Larger particle size (from low electrophoretic velocity) produces much lower Brownian velocity (extending the collision time with the film), which, along with the extant thermophoretic force, will cause the packing density of the film to increase.

Now, if particles were equally positively and negatively charged, then the packing density should have been symmetric about the 0 V. However, from the Figure 5.4 we can see that the packing density is lower at negative voltages of |-200 V| and |-400 V| than at the positive voltages of the same magnitude. The TEM images in Figure 5.3 show that the average primary particle size at a voltage of -400 V is much less than that at +400 V, meaning the particles undergo less in-flame agglomeration at -400 V than at +400 V. This shows that a negative voltage applied on the substrate has more influence on the particles than a positive voltage. So they will be more attracted to a negative substrate than to a positive substrate explaining the lower size of the particles at -400 V. Thus, this result concludes that more particles are positively charged than negatively charged, due to thermionic emission. This also explains why -400 V is the lowest point (due to smallest particles) at which the packing density is minimum, and the film has a high porosity.

5.3 CASE 2:
Precursor concentration – 116 ppm
Substrate temperature – 663 K
Synthesis time – 300 seconds

5.3.1 Introduction

Case 2, similar to case 1, has the TTIP concentration set at 116 ppm. The substrate temperature for this case is increased to 663 K. The temperature of the substrate is increased by increasing the thickness of the quartz blocks between the aluminum plate and cooling plate and decreasing the flow rate of cooling water. As the precursor concentration is still 116 ppm, the time for the synthesis of each experiment is 300 seconds. The substrate temperature is measured by a K-type thermocouple. It remains constant at 663 K throughout the experiment with an accuracy of $\pm 10^{o}$C.

5.3.2 Results

5.3.2.1 SEM

Figure 5.5 shows SEM images of cross-sections of TiO_2 films grown in the SSF without applying an electric field and under the effect of voltages from -800 V to +800 V. The thickness of the films is around 37-40 μm. Image for 0V shows an SEM image of the titanium oxide film when there is no electric field applied to the substrate. The film still shows the same tree-like branched structure as seen in case 1 for the film formed in the absence of an electric field (Figure 5.1 image 0 V). However, the nanoparticles at the

base of the film in this image seem agglomerated. As the temperature of the substrate is high, the particles sinter on the surface of the substrate to form larger agglomerates. The growth of the nanoparticles in the film is prominent in the horizontal direction which results in more branches. The structure of the film is also similar to that of the TiO_2 film shown by Zhang et. al[42] in his paper formed under the same substrate temperature and precursor concentration. The growth of the nanoparticles in the film at 0 V is more prominent in the horizontal direction than in the films formed under a voltage, corresponding to more branched structures. The structure in the images for -200 V, +200 V, -400 V, and +400 V shows a more columnar growth of the particles. The film at -400 V as can be seen from the image is highly porous as compared to the other films in the figure with a very small particle size. The films look more packed in the images for -600 V, +600 V, -800 V, and +800 V with a higher particle size as compared to the earlier images. Further explanation for the growth and structure of the films will be discussed in the later section.

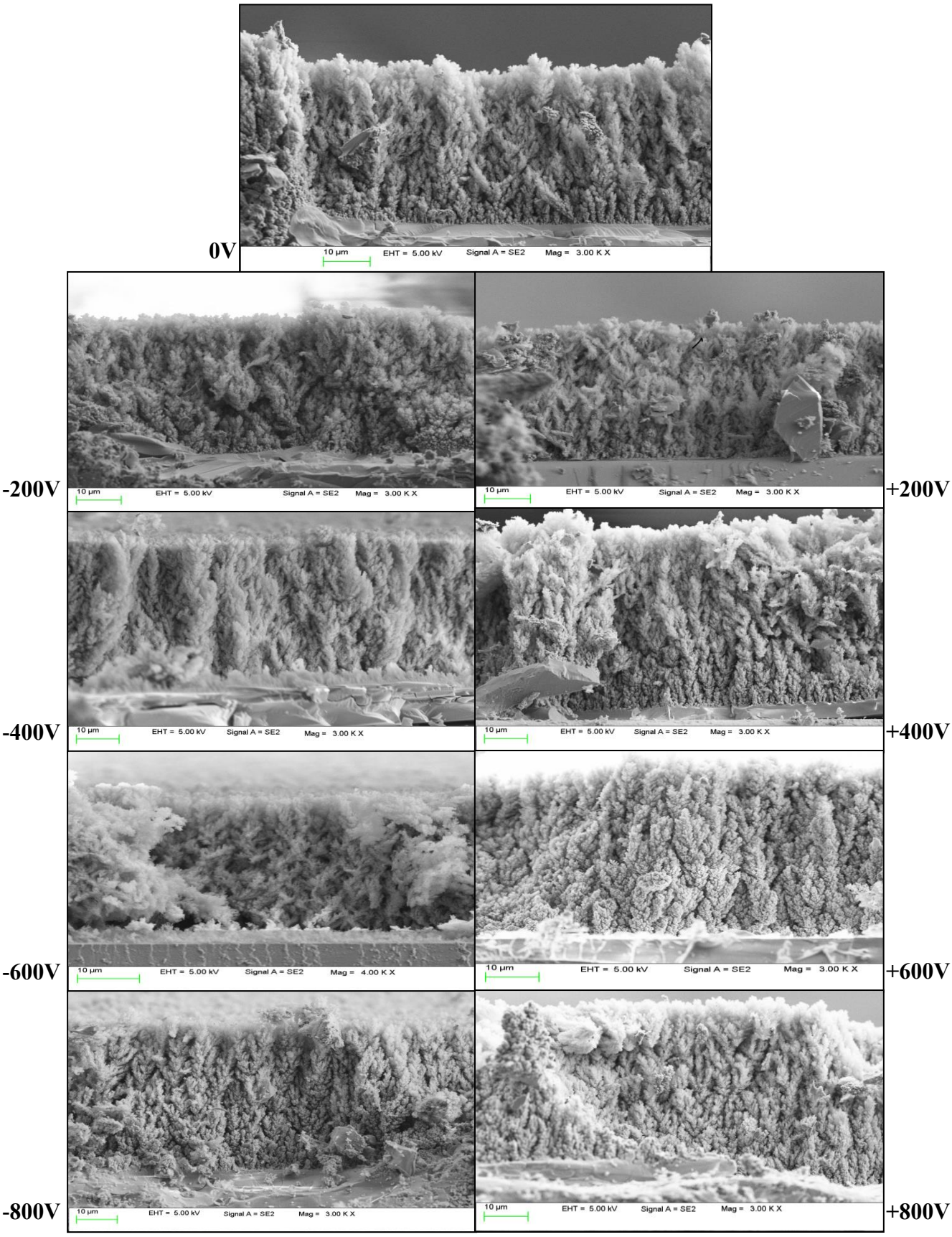

Figure 5.5. SEM images of the TiO_2 films for CASE 2.

5.3.2.2 Packing Density

Figure 5.6 shows the graph of packing density of the nanostructured TiO_2 films for case 2 under applied voltages from -800 V to +800 V. The trend shows that the packing density of the films is less under lower voltages until |±400 V| after which there is an increase until |±800 V|. The packing density of the films agrees with their respective SEM images in figure 5.5. The images for 0 V, -200 V, and +200 V in figure 5.5 show a similar packing of the particles in the film. This can be confirmed from the packing densities for 0 V, -200 V, and +200 V, which are quite close to each other. The highest packing density between the three is at 0 V. The packing density of the film at -200 V is less than that at +200 V. The image for -400 V shows a high porosity of the film which can be confirmed from the trend of the packing density in the graph showing a minimum value at -400 V. The packing density of the film at +400 V is lower than that at 0 V but it is still higher compared to that at -400 V. The packing density increases at higher voltages of |± 600 V| and |± 800 V|. The packing density at +600 V is peculiarly the highest which can be confirmed from the SEM image for the same. The film here is highly packed and the particle size is also much larger compared to all the other films.

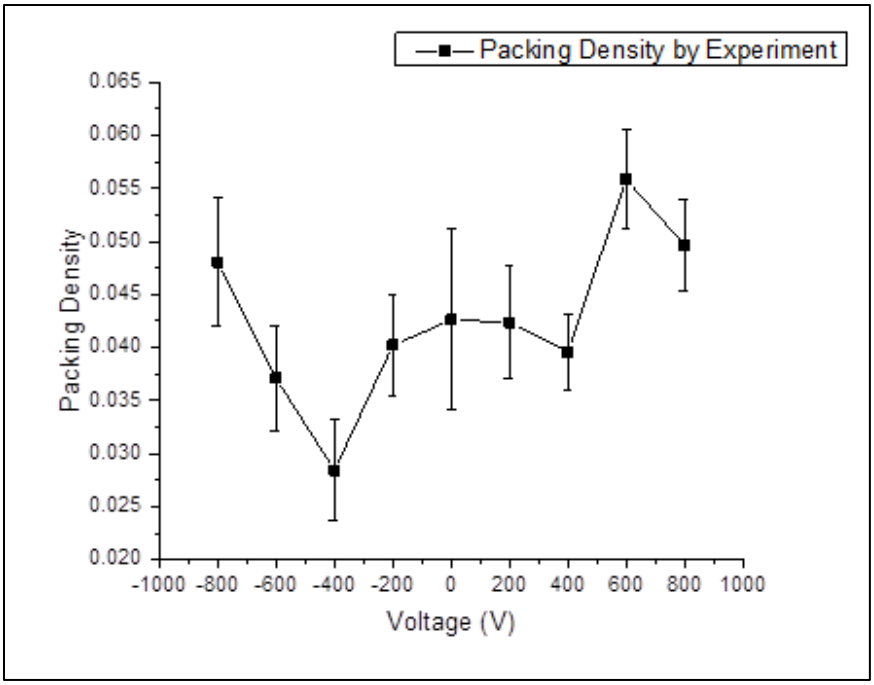

Figure 5.6. Packing Density of the TiO_2 film for case 2 under a voltage from -800 V to +800 V by experiment.

5.3.3 Discussion

In the absence of an electric field applied to the substrate, the main forces acting on the particles affecting their structure in the film are the thermophoretic effect and Brownian motion. The thermophoretic effect is responsible for the growth of the film in a vertical direction while the Brownian motion causes the movement of the nanoparticles in a horizontal direction resulting in a branched structure. The packing density of the TiO_2 films grown in an SSF without applying any electric field is a result of this horizontal movement due to the Brownian motion and the penetration depth of the film affected by the thermophoretic velocity.

When an external electric field is applied to the substrate, it will affect the deposition and growth of the particles. In addition to thermophoresis and Brownian motion, an electrophoretic effect will act on the particles, impacting the structure of the film. As discussed in section 5.2.3, the two regimes affecting the particles in the SSF under an external electric field are the electrophoretic velocity and the average size of the primary particles in the flame incident on the film. Under lower voltages up to |±400 V|, the charged particles are attracted to the opposite polarity fields. The electrophoretic velocity should aid the thermophoretic velocity of the particles causing them to penetrate deeper into the film. However, the particles have smaller average size as they spend less time in the flame, and the nuclei of the particles have less time to grow, which impacts the collision time through increase in the Brownian velocity. This combined effect ends up decreasing the packing density of the films. Conversely, under higher voltages up to |±800 V|, the particles undergo strong molecular collisions to form positive ions and electrons. Depending on the polarity of the substrate, either the positive ions (for a positive voltage on the substrate) or the negative ions (for a negative voltage on the substrate) will attach to the particles giving them a net positive or negative charge. These incoming particles are then repelled from the surface of the substrate decreasing the electrophoretic velocity but increasing the size of the particles incident on the film as they spend more time in the flame. Here, the larger particle size corresponds to lower Brownian velocity, increasing the characteristic time before collision of the incoming particle with the particles in the film, which outweighs the effect of decreased electrophoretic velocity. Thus, the packing density will increase resulting in a film with less porosity. Again, the packing density of the TiO_2 films under negative voltages of |-

200 V| and |-400 V| is less than under positive voltages of the same magnitude, confirming that more particles are positively charged than negatively charged due to the thermionic emissions. These positively charged particles attract to the substrate under a negative voltage reducing the residence time in the flame and repel from the substrate under a positive voltage increasing the residence time in the flame, which will decrease or increase the packing density respectively.

5.4 CASE 3:
Precursor concentration – 116 ppm
Substrate temperature – 763 K
Synthesis time – 300 seconds

5.4.1 Introduction

The substrate temperature for case 3 is increased to 763 K. To obtain this high temperature, the distance between the cooling plate and aluminum plate is increased by adding a thickness to the quartz blocks and decreasing the flow rate of cooling water to minimum. The temperature of the substrate is confirmed to be 763 K ± 10^{o}C using a pyrometer. During the experiments, a K-type thermocouple continuously monitors the substrate temperature. As the precursor concentration is same as in earlier cases 1 and 2, the synthesis time is still 300 seconds.

5.4.2 Results

5.4.2.1 SEM

Figure 5.7 shows SEM images of the cross-section of TiO_2 films grown in the SSF without applying the electric field and under the effect of applied voltages from -800V to +800 V. The thickness of the films is around 35-38 μm. Image for 0 V shows an SEM image of the titanium oxide film when there is no electric field applied to the substrate. The structure of the film is also similar to that of the TiO_2 film shown by Zhang et. al[42] formed under the same substrate temperature and precursor concentration. The structure of the film seems more branched in the horizontal direction. Also, the particles are more agglomerated. The temperature of the substrate for this case is very high (763 K). Such a high temperature of the substrate will result in increased on-substrate sintering of the titanium oxide nanoparticles, which will result in large agglomerates in the film structure. The growth and structure of the nanoparticles seen in the images for -200 V, +200 V, -400 V, and +400 V is similar to the structure seen in the images of the films under same electric field for the earlier cases 1 and 2. It can be seen that the film is more porous and the particle size looks smaller under the application of negative voltages of |-200 V| and |-400 V|, while the film is more packed with higher particle size under the application of positive voltages of |+200 V| and |+400 V|. The images for -600 V, +600 V, -800 V, and +800 V follow the trend as seen in earlier cases where the film becomes less porous and the particle size increases under the application of higher electric fields.

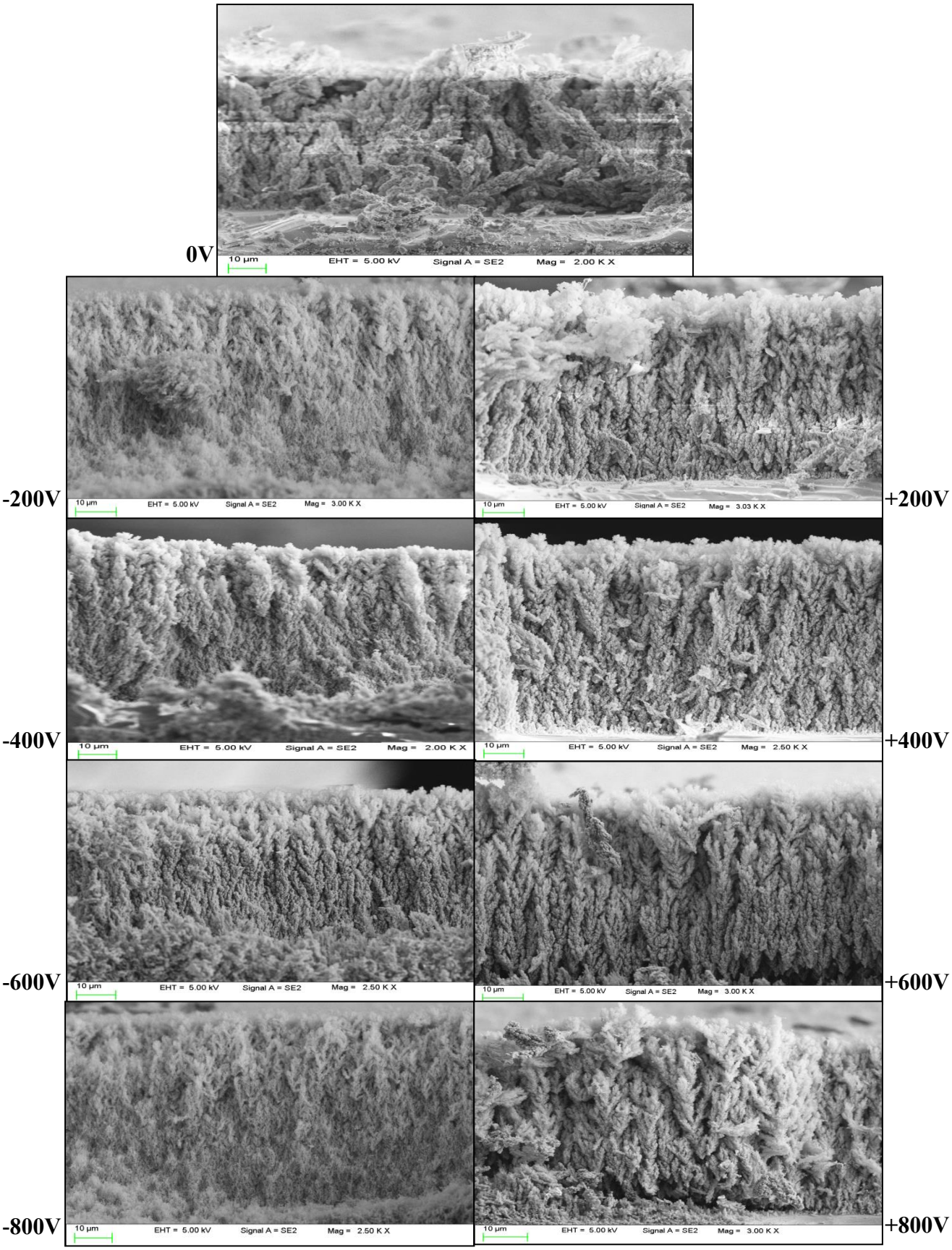

Figure 5.7. SEM images of the TiO_2 films for CASE 3.

5.4.2.2 XRD

Figure 5.8 shows the XRD analysis of the titanium oxide nanoparticles taken from the surface of the film. The analysis confirms that the phase of the particles is still anatase. Thus, the particle phase remains unaffected by the electric field applied and is independent of the strength of electric field.

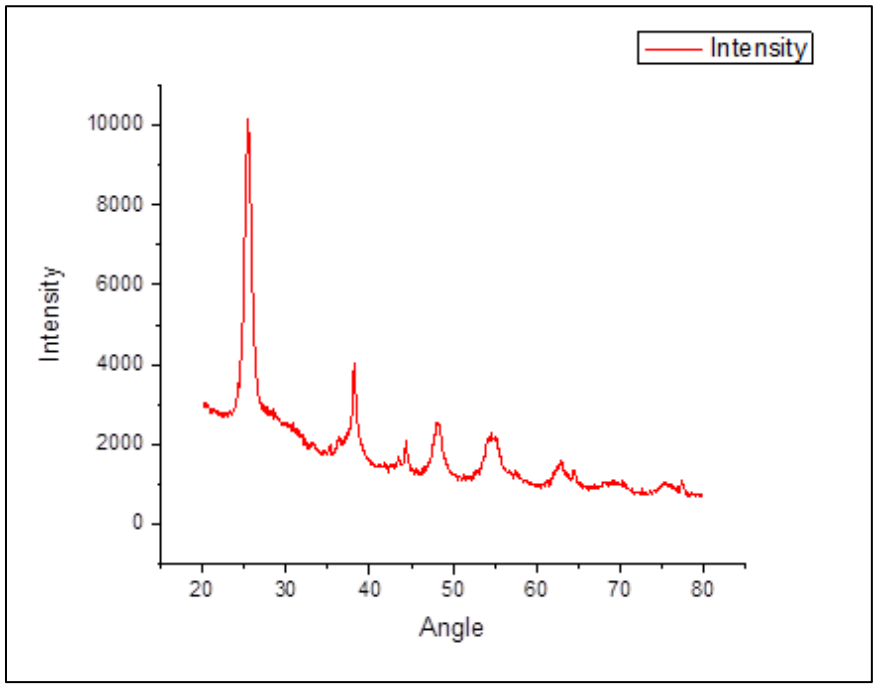

Figure 5.8. XRD analysis of the TiO_2 nanostructured film in the absence of electric field for case 3.

5.4.2.3 TEM

Figure 5.9 shows the TEM images of the titanium oxide nanoparticles from the surface of the film grown in a SSF without any applied voltages, under a voltage of -400 V, and under a voltage of +400 V. The size of the particles seen in the images obtained from

TEM can be measured by a program called Digital Micrograph. About 20-30 particle diameters are measured from each image and an average is calculated to obtain the average primary particle size. This will be the same as the average primary particle size of the titanium oxide particles in the film.

The average diameter of the particles in the image for 0 V was found to be 10 nm, while that in the image for -400 V was found to be about 8-9 nm. The average diameter of particles in the image for +400 V was measured to be 12nm. It can also be seen from the images that the size of the particles at -400 V is much smaller compared to 0 V and +400 V. This agrees with the average diameter of the particles calculated by Digital Micrograph program. Thus, the particles in the film formed under a voltage of -400 V are smaller in size than those formed under no electric field. The particles at +400 V are larger than those formed under no electric field. This confirms the trend seen in the TEM images of case 1. It also agrees with the theory discussed in section 5.2.3.

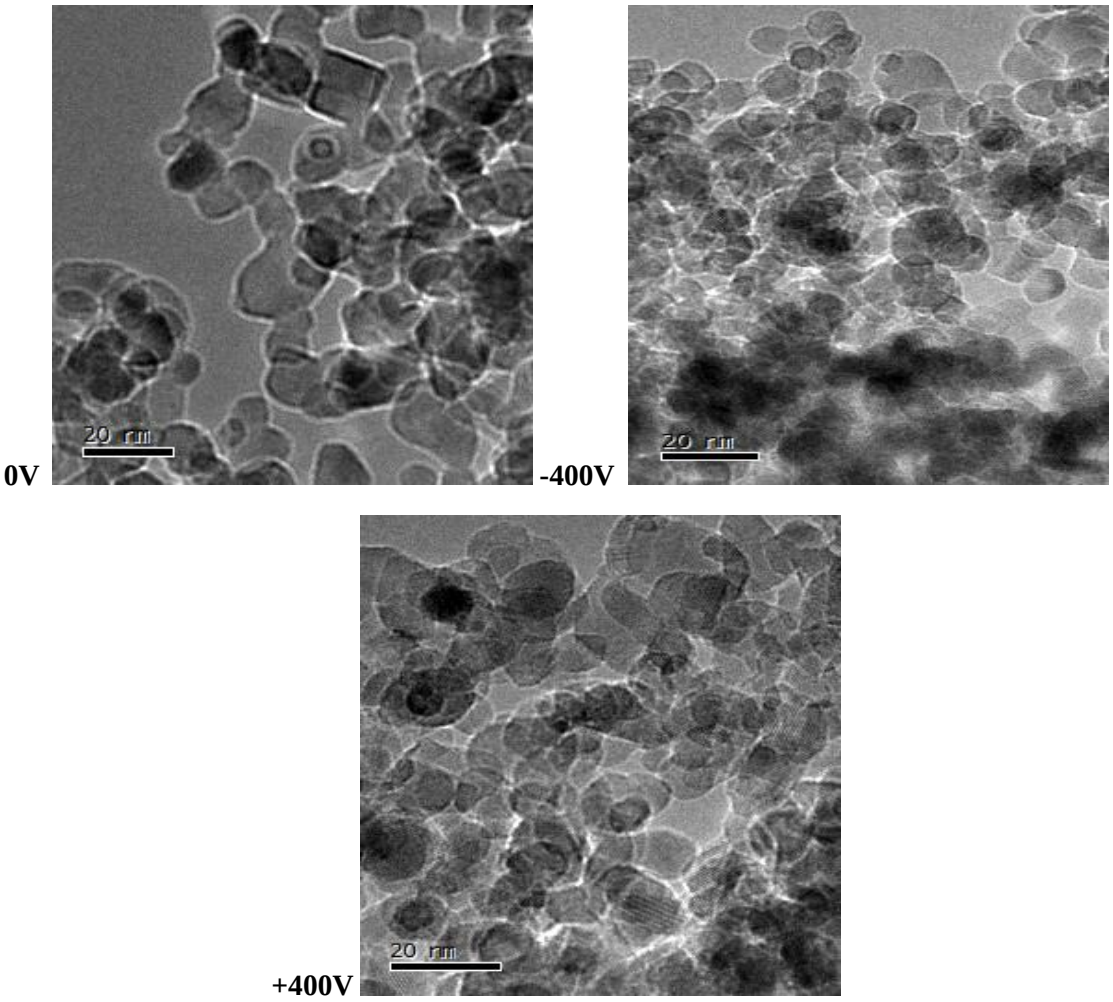

Figure 5.9. TEM images of TiO_2 nanoparticles for case 3.

5.4.2.4 Packing Density

Figure 5.10 shows the graph of packing density of the TiO_2 films for all the 9 experiments from -800 V to +800 V including 0 V. The figure shows the trend of packing density calculated both by experimental methods and by correlation of the deposition model of the particles on the film. The trend seen in the figure is similar to the trends of packing density that were seen in the earlier cases 1 and 2. The TiO_2 film under the

voltage of -400 V still has the least packing density which means it is the most porous compared to the films grown under other electric fields. The increase in the packing density of the films can be seen at higher electric fields thus agreeing with the trends in earlier cases.

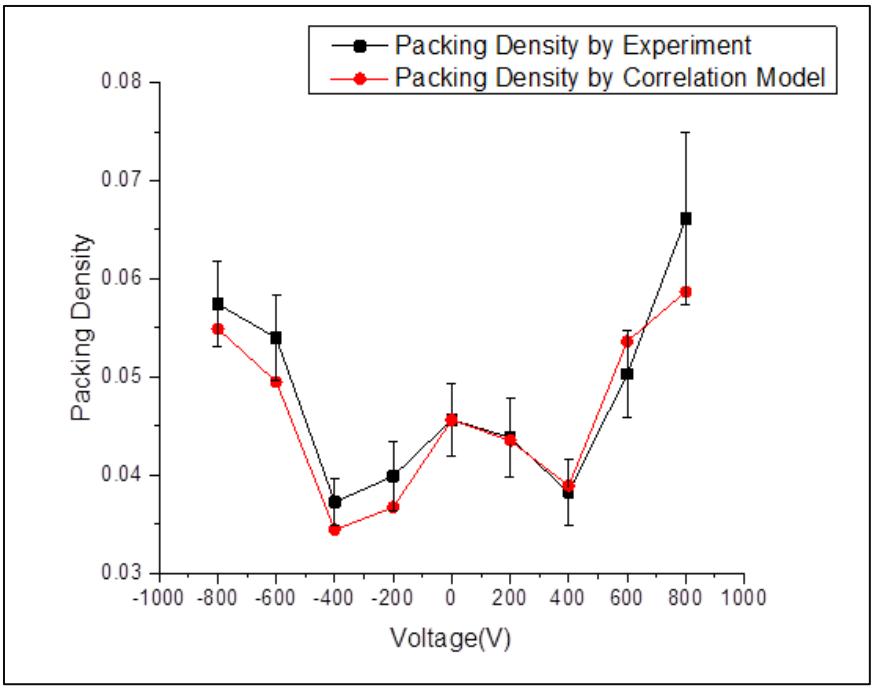

Figure 5.10. Packing Density of the TiO_2 film for case 3 from -800 V to +800 V by experimental and model calculations.

5.4.3 Discussion

The deposition and growth of the particles on the silicon substrate can be explained by the same theory discussed in sections 5.2.3 and 5.3.3. The electrophoretic velocity and thermophoretic velocity will affect the penetration of particles in the film. As the temperature of the substrate is very high (763 K), the temperature gradient between the

burner and the substrate is reduced. This will decrease the thermophoretic velocity thus slowing down the nanoparticles incident on the film. At the same time an increased rate of sintering on the substrate due to the high temperature will cause the particles to agglomerate increasing their size. The combined effect of these two situations along with the Brownian motion will affect the packing density of the films in the absence of any electric field.

The TEM images show a smaller size of the particles at -400 V and a larger size at +400 V. This demonstrates that the particles in the film for a negative field are smaller in size compared to the particles for a positive electric field. So, the particles in a negative electric field spend less time in the flame causing their size to be smaller. Thus, the nanoparticles must be more attracted and affected by a negative electric field than a positive one at lower electric field strengths, meaning that more particles are positively charged. At higher voltages applied to the substrate, due to molecular collisions which form positive ions and electrons, the particles will gain a net positive or negative charge. This charge on the particles will be the same as the polarity of the voltage on the substrate causing them to repel back into the flow field, thus increasing the particle residence time in the flame. As a result, in spite of a low thermophoretic velocity which would cause the particles to slow down, the larger particle size due to more in-flame agglomeration will cause the packing density of the films to increase at higher electric field strengths.

5.5 Comparison of Packing Density for Cases 1, 2, 3

Figure 5.11 below shows the graph of packing density of the nanostructured films for cases 1, 2 and 3 grown when there is no electric field applied to the substrate. The graph shows the packing density first decreases as the temperature increases from 473 K to 663 K after which it again increases at 763 K. The trend of the graph is similar by both experimental and correlation calculation. As discussed the thermophoretic velocity of the particles affects their penetration depth into the film. At a low substrate temperature, the thermal gradient between the substrate and the burner will be high, increasing the thermophoretic velocity acting on the particles. Thus, the particles will penetrate deeper into the film causing the film to be more packed which can explain the higher packing density. As the temperature increases, the temperature gradient decreases, thus slowing the particles down. This will decrease the penetration of particles in the film which would loosen the film causing the packing density to decrease. As the temperature increases further to 763 K, the temperature gradient will further decrease which should decrease the packing density further. However, at such a high substrate temperature, the particles will sinter on the substrate to form larger agglomerates. The larger agglomerates of the particle will form a more packed film. The combination of lower thermophoretic velocity and on-substrate sintering will result in an increase in the packing density of the film.

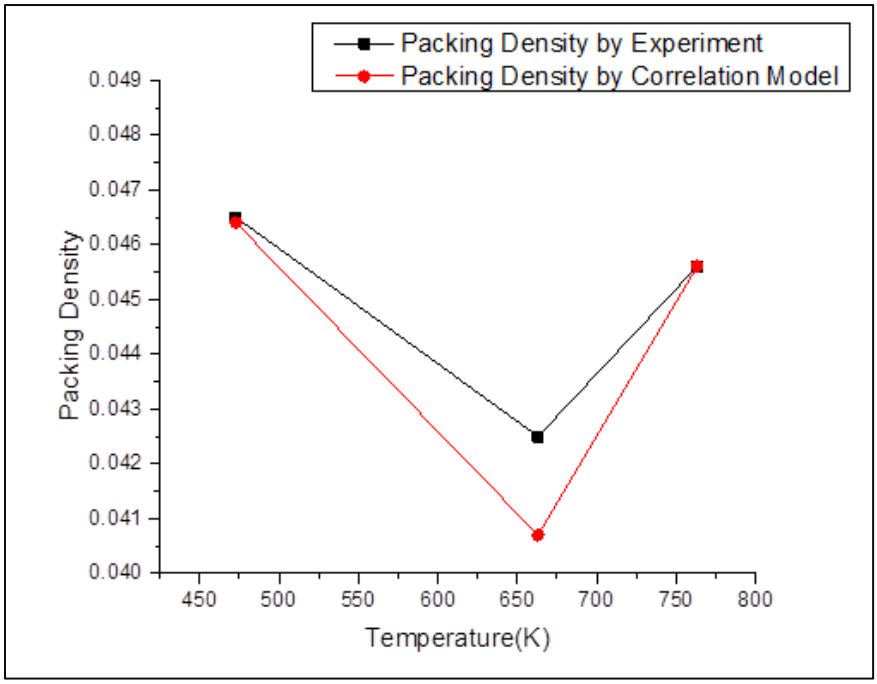

Figure 5.11. Graph of Packing Density versus Substrate Temperatures 473 K, 663 K and 763 K at constant precursor concentration of 116 ppm.

CHAPTER 6

EFFECTS OF ELECTRIC FIELD AND PRECURSOR CONCENTRATION

6.1 Introduction

This chapter deals with the study of the last four cases in table 2.2. In this chapter, the substrate temperature is kept constant at 763 K for all the four cases. The precursor concentration is varied from 29.1 ppm to 291 ppm. The four precursor concentrations which are studied in the cases are: 29.1 ppm, 116 ppm, 232.8 ppm, and 291 ppm. As we have already studied the case with the substrate temperature of 763 K and precursor concentration 116 ppm in case 3, section 5.4, it will not be discussed again. Each case has 9 set of experiments:

1. No electric field applied or 0 V
2. -200 V
3. -400 V
4. -600 V
5. -800 V
6. +200 V
7. +400 V
8. +600 V
9. +800 V

The precursor concentration is varied by changing the N_2 carrier gas flow rate and the temperature at which the precursor is heated. In spite of the concentration of TTIP in the burner differs, the total amount of TTIP added during an experiment should be the same. Thus, when the TTIP concentration is low, the synthesis time will increase and when the concentration is high, the synthesis time will decrease. This ensures the total precursor added remains the same.

Below, each case is discussed for the above experiments and their results.

6.2 CASE 4:
Precursor concentration – 29.1 ppm
Substrate temperature – 763 K
Synthesis time – 1200 seconds

6.2.1 Introduction

In this case, the TTIP concentration is set at 29.1 ppm. This is achieved by adjusting the N_2 carrier gas flow rate to 10% of the total flow rate from the mass flow controller and keeping the bubbler heating at 80^oC. The substrate temperature is kept constant at 763 K. As the precursor concentration in the bubbler is very low, the synthesis time is longer, to ensure the same total mass of precursor delivered. The experiment synthesis time is 1200 seconds. A voltage is applied to the substrate to study the effect of electric field on the growth and structure of the titanium oxide films. A set of 9 experiments with voltages ranging from -800 V to +800 V are conducted. The results of the experiments are presented below.

6.2.2 Results

6.2.2.1 SEM

Figure 6.1 shows the SEM images of cross-section of nanostructured titanium oxide films for the above substrate temperature and precursor concentration. The image for 0 V shows the TiO_2 film formed in the absence of an electric field. As can be seen from the image, the tree like branched structure of the films seen in earlier cases for the same 0 V is absent in this film. The main reason for this is the very low concentration of TTIP[42]. Due to the very low precursor concentration, the amount of particles in the flame incident on the film is very low. The substrate temperature is very high so the temperature gradient between the substrate and the burner is low, decreasing the thermophoretic velocity. The smaller number of particles and the lower thermophoretic velocity are not enough to give a structure to the film as seen in earlier cases, resulting in a clustered formation of the particles on the film instead of the tree-like branched structure. Also, the very high temperature of the substrate will cause the low number of particles to sinter on the film forming larger agglomerates. The smaller concentration of TTIP also results in a very low thickness of the film only around 20-25 μm. As the electric field is applied to the substrate, the branched structure starts becoming visible again in the films. In the images for -200 V, +200 V, -400 V, and +400 V the branched structure of the film seen in earlier cases is visible. The thickness of the film is also a little higher, around 30μm. However, the particles still seem to be agglomerated due to the on-substrate sintering. The reason for this columnar and branched structure in the films is the long synthesis

time and low concentration of TTIP resulting in sintering of the particles in the film. Also, the low TTIP concentration will make it difficult for the particles to homogenously nucleate in the flow field. Similarly, the films in the images for -600 V, +600 V, -800 V, and +800 V show the columnar and branched structure of the film. The structure also seems to have longer “branches” and the thickness of the films is again low.

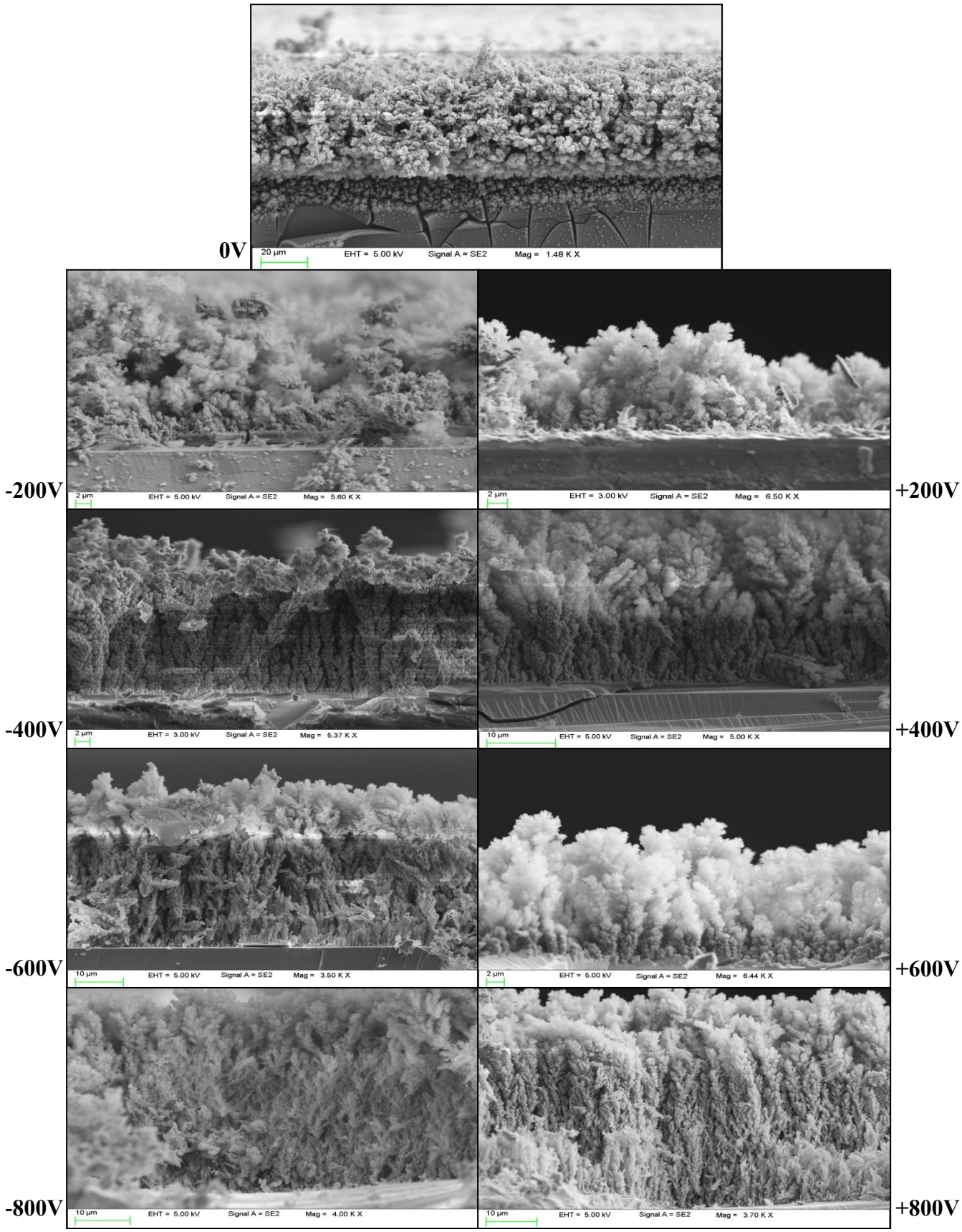

Figure 6.1. SEM images of the TiO_2 films for CASE 4.

6.2.2.2 XRD

Interestingly, the phase of the TiO_2 particles in the films for case 4 is found to be a mixture of anatase and rutile. The analysis in Figure 6.2 shows the particles have a small percentage of rutile. The rutile percent in the particles in the absence of any electric field is 18.5% while the anatase content is 81.5%.This is due to the long synthesis time of the experiment, resulting in a long annealing time of the film on the substrate. This would cause a small amount of particles in the film to change their phase to rutile on the substrate.

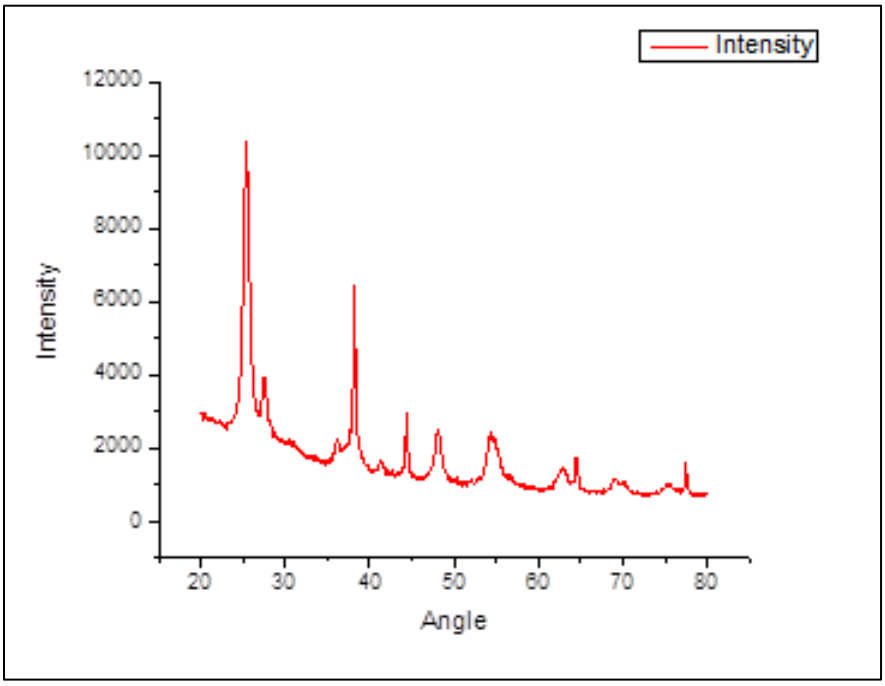

Figure 6.2. XRD analysis of the TiO_2 nanostructured film in the absence of electric field for case 4.

6.2.2.3 Packing Density

Figure 6.3 shows the trend of packing density of the TiO_2 films for case 4 under an applied voltage from -800 V to 800 V. The trend on the negative side from -200 V to -800 V is similar to the earlier cases where the packing density is minimum at -400 V. The SEM images of the films corresponding to the voltages confirm the packing densities seen in the figure 6.3. The trend on the positive side is slightly different than that seen in the earlier cases as the packing densities for +200 V and +400 V are higher than that for 0 V unlike seen in cases 1, 2, and 3. However, from +600 V, the trend of high packing density is similar to the earlier cases. The reason for these packing densities is discussed in the section below

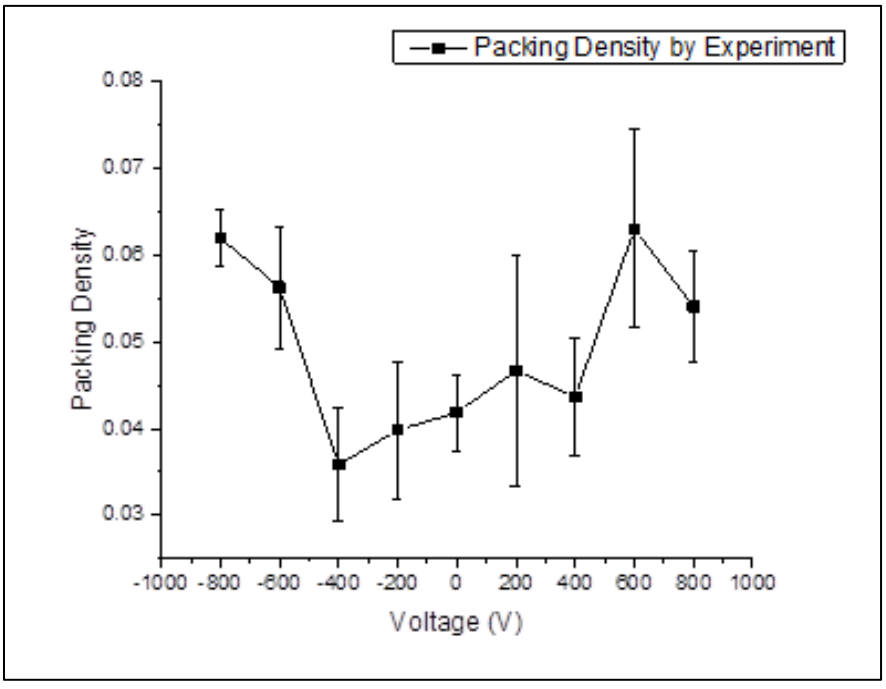

Figure 6.3. Packing Density of the TiO_2 film for case 4 under a voltage from -800 V to +800 V by experiment.

6.2.3 Discussion

The average particle diameter of the nanoparticles for a low precursor concentration is less than that at higher concentration[41,54,55]. As a result, the packing density which is dependent on the average size of the particles incident on the film for 0 V is low. When a low negative voltage is applied like |-200 V| or |-400 V|, the electrophoretic velocity will add to the thermophoretic velocity increasing downward velocity of the particles and the penetration depth. However, at the same time due to low in-flame agglomeration added to the already low particle diameter will lower it further. As a result, is spite of the on-substrate sintering the packing density of the films will be lower than that at 0 V. When a low positive voltage is applied up to |+400 V|, the attraction of the particles to the substrate is not as strong due to the charge on the particles being more positive than negative, due to thermionic emission. Hence, the particles will not have the same electrophoretic velocity acting on them as when a negative field of the same strength is applied. Thus, the particle diameter will be slightly larger at +200 and +400 V as compared to that at -200 and -400 V. Thus, the packing density will be higher. However, the packing density at 200 and 400 V seems to be higher than that at 0 V as well unlike the cases 1, 2, and 3. At low voltages on the substrate, the magnitude of the voltages is not enough to cause collisions of the particles. As a result, the positive ions and electrons in the flame are less and do not affect the charge on the particles much. However, due to the thermionic emissions, more particles are positively charged. These particles will repel from the substrate back into the flow field. Thus, they will stay in the flame longer increasing the primary particle size. As the nucleation of the particles at 0 V is very low

due to low TTIP concentration, the primary particle size at +200 V and +400 V is much higher than that at 0 V. Thus, the packing density at these voltages is higher than that at 0 V. At higher voltages like ± 600 V and ± 800 V, the particles will be repelled from the surface of the substrate because of the same charge of particles and the voltage on the substrate as explained in earlier cases. As a result, the higher particle size due to in-flame agglomeration, and the decreased Brownian velocity (or increased collision time) will increase the packing density of the films.

6.3 CASE 5:
Precursor concentration – 232.8 ppm
Substrate temperature – 763 K
Synthesis time – 150seconds

6.3.1 Introduction

In this case, the TTIP concentration is set at 232.8 ppm. This is achieved by adjusting the N_2 carrier gas flow rate to 40% and keeping the bubbler heating at 100^oC. The substrate temperature is kept constant at 763 K. The experiment synthesis time is 150 seconds. A voltage is applied to the substrate to study the effect of electric field on the growth and structure of the titanium oxide films. A set of 9 experiments with voltages ranging from -800 V to +800 V are conducted. The results of the experiments are shown below.

6.3.2 Results

6.3.2.1 SEM

Figure 6.4 shows the SEM images of the cross-section of nanostructured TiO_2 films under different applied electric fields for a substrate temperature of 763 K and precursor concentration of 232.8 ppm. The image for 0 V shows the film grown in the SSF in the absence of any external electric field. The thickness of the film is about 45-50 μm. Also, from the image we can see that the film is more packed compared to the earlier cases. The reason for both the high thickness and high packing is the increased concentration of TTIP delivered to burner[42]. This increased concentration will promote homogeneous nucleation and increase the number of particles in the flame incident on the substrate to form a film. However, we can still see the branched structure of the film as in earlier cases. In the images for -200 V, +200 V, -400 V, and +400 V we can see the columnar structure of the films formed under the effect of an external electric field. The high substrate temperature will lead to some on-substrate sintering of the nanoparticles inside the film to form larger agglomerates. In spite of this, the films formed under -200 and -400 V still show a porous structure composed of small particles compared to their counterparts in images for +200 V and +400 V. The size of the particles inside the films at -800 V and +800 V seems much smaller as compared to in the earlier cases for the same voltage magnitudes. All the films in the images have quite high thickness of an average 48 μm due to the high concentration of TTIP.

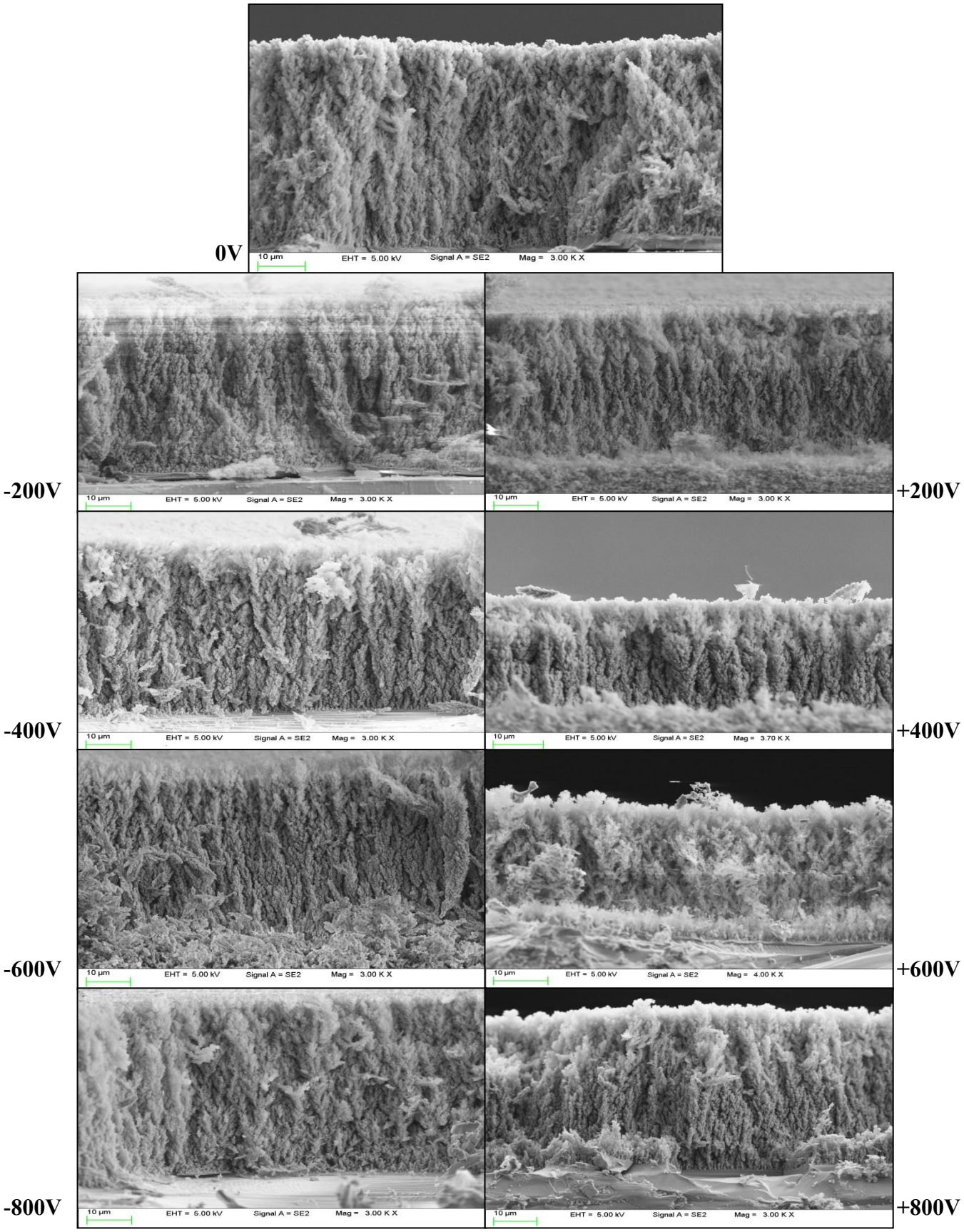

Figure 6.4. SEM images of the TiO_2 films for CASE 5.

6.3.2.2 Packing Density

Figure 6.5 shows the graph of packing densities of the TiO_2 films under voltages from -800 V to +800 V. The trend is similar to that seen in earlier cases for the positive and negative electric fields. However, in this case, the packing density of the film at 0 V, which is in the absence of any electric field, is highest of all and even higher than at ±800 V. The only reason for this is the high precursor concentration which will be explained in detail in the next section. The trend shows the packing density of the film is still the least at -400 V, like in all the other cases. Thus -400 V still has the most influence on the particles in the flame. However, after a closer look, it seems the packing densities of the films at higher voltages of ±600 V and ±800 V are not as high as seen in the earlier cases. In fact, the packing densities for these voltages are less than the packing density at 0 V.

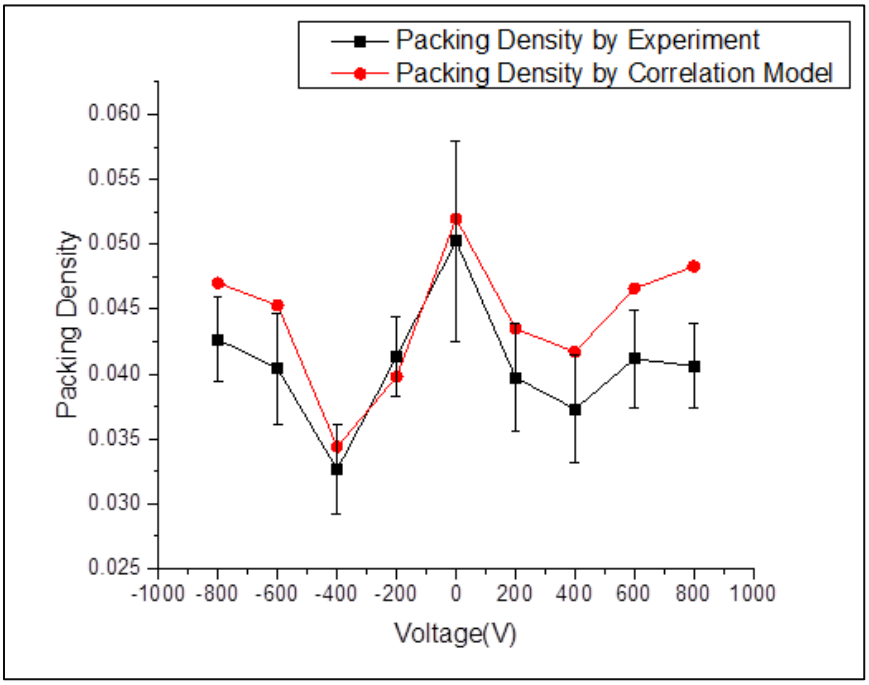

Figure 6.5. Packing Density of the TiO_2 film for case 5 under voltages from -800 V to +800 V by experiment and model calculation.

6.3.3 Discussion

As seen in figure 6.5 above the packing density of the film in the absence of an electric field is very high. As stated before, when the precursor concentration is increased, a larger amount of particles are formed in the flame. The primary particles coagulate, thus increasing the size of their nuclei. This results in the increase of average primary particle diameter for particles incident on the film[41]. As the average primary particle size affects the packing density, increase of the size will create a more packed film. As observed above, the packing densities at higher voltages are not as high as those for the same voltages in the earlier cases. Now this is an anomaly as in all the earlier cases we have seen that the packing densities of the films are highest under the voltages of ±600 V and ±800V. When a high voltage is applied to the substrate, positive ions and electrons are formed due to molecular collisions. Depending on the polarity of the applied voltage, the positive ions will attract to the negative voltage on the substrate or the electrons will attract to the positive voltage on the substrate. Thus, the oppositely charged ions will attach to the particles in the flow field making them of the same charge as that on the substrate. These particles will repel back into the flow field. But, now because of the high TTIP concentration in the flame and the strong electric field, the flame structure will be affected. Thus, the particles will move inside the flame reducing the in-flame agglomeration and the primary particle size. So, when the particles finally deposit in the film, they are not as agglomerated which will reduce the packing density of the film.

6.4 CASE 6:
Precursor concentration – 291ppm
Substrate temperature – 763 K
Synthesis time – 120seconds

6.4.1 Introduction

In this case, the TTIP concentration is set at 291 ppm. This is achieved by adjusting the N_2 carrier gas flow rate to 45% and keeping the bubbler heating at 100^oC. The substrate temperature is kept constant at 763 K. As the precursor concentration in the bubbler is high, the synthesis time is shorter. The experiment synthesis time is 120 seconds. A voltage is applied to the substrate to study the effect of electric field on the growth and structure of the titanium oxide films. A set of 9 experiments with voltages ranging from -800 V to 800 V are conducted. The results of the experiments are shown below.

6.4.2 Results

6.4.2.1 SEM

Fig 6.6 shows the SEM images of the cross-section of nanostructures titanium oxide film for case 6 with substrate temperature 763 K and precursor concentration 291 ppm under the effect of voltages from -800 V to +800 V. The image for 0 V shows the SEM image of the film when there is no electric field applied to the substrate. From the image, it is visible that the tree-like branched structure present in the earlier cases is absent in the film for this case. As the precursor concentration is very high, the concentration of TiO_2 particles in the flame is very large. As a result, the particles are not deposited in the

typical branched structure that we saw in the earlier cases[42]. However, as the electric field is applied, the branched structure of the film slowly starts to develop as seen from the images for -200 V, +200 V, -400 V, and +400 V. The films at -200 V and -400 V show a columnar structure with less branching and more growth in the vertical direction as previously seen in the earlier cases for same electric fields. The films seem to have less particle agglomerates and more porosity. The average thickness of the films is about 30 μm. Conversely, the films grown under the voltages of positive |+200 V| and |+400 V| seem to be more packed, although the columnar structure is still visible. As the voltage increases to ±600 V and ± 800 V, the structure of the films changes a little compared to that under lower voltages. The film at -600 V doesn't clearly show the columnar structure present in the other images. Also, the particles seem to be more agglomerated. The film at +600 V has a more branched structure while the films at ±800 V show a columnar structure. The films at ± 800 V looks more packed, and the structure is more distorted at a few places and not consistently columnar.

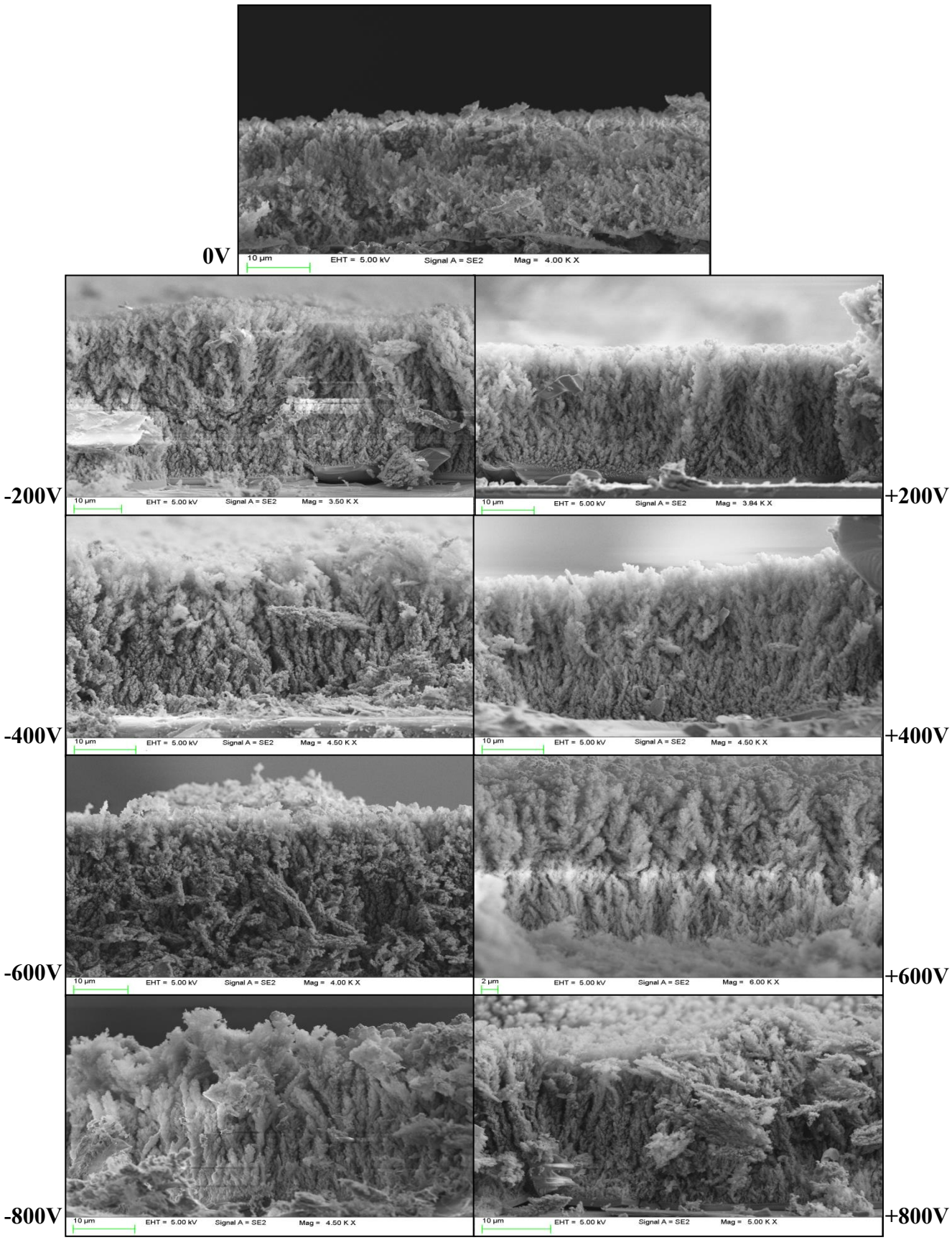

Figure 6.6. SEM images of the TiO_2 films for CASE 6.

6.4.2.2 Packing Density

Figure 6.7 shows the graph of packing densities of the TiO_2 films under voltages from -800 V to +800 V. The trend is similar to that seen in earlier cases for the positive and negative electric fields. Similar to the earlier case 5, the packing density of the film in the absence of any electric field is maximum as compared to the packing densities under applied voltages. The reason for this is again perhaps the very high precursor concentration increasing the average primary particle size incident on the film. Thus, the film becomes highly packed and loses its porosity. The trend shows the packing density of the film is still the least at -400 V, like in all the other cases. Thus, -400 V is most effective on decreasing the packing density of the films. Similar to the case 5, the packing densities of the cases ± 600 V and ±800 V are smaller than that at 0 V. The reason for this is discussed in the next section.

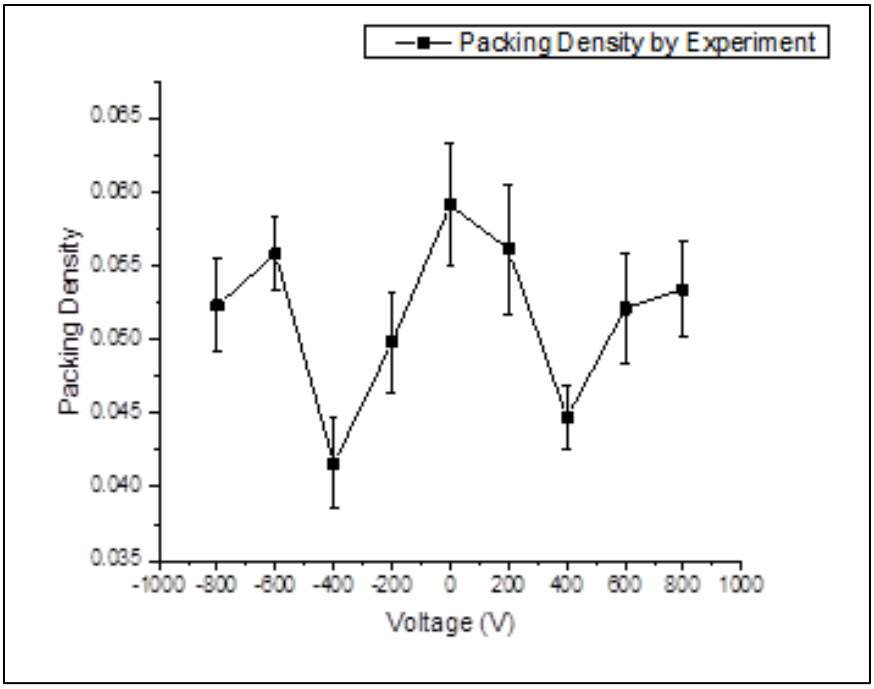

Figure 6.7. Packing Density of the TiO_2 film for case 6 under voltages from -800 V to +800 V by experiment.

6.4.3 Discussion

As discussed in the previous case 5, the high precursor concentration results in a high primary particle size incident on the film[41,54,55]. This causes the film at 0 V to lose its branched structure. As the temperature gradient is low, the thermophoretic velocity is also reduced. As a result the particles will move downward slower. However, the high particle size owing to the high precursor concentration results in a high packing density at 0 V. The anomaly found in case 5 is also seen in this case as the packing densities at higher field strengths are not higher than the packing density at 0 V. In all the earlier cases we have seen that the packing densities of the films are quite high under the voltages of ±600 V and ±800 V and even higher than at 0 V. The anomaly can again be

explained by the high TTIP concentration. The high voltage on substrate causes the particles to have the same charge as that of the voltage applied. The particles repel from the substrate and stay longer in the flame. However, due to the high TTIP concentration and high electric field in the flame, the flame structure is affected causing the particles to move inside the flame. As a result, the particles do not agglomerate as much resulting in a lower agglomerate size of the particles in the film, decreasing the packing density.

6.5 Comparison of Packing Density for Cases 3, 4, 5, 6

Figure 6.8 shows the graph of precursor concentration versus the packing density. The trend of the packing density of the TiO_2 films at 0 V as the precursor concentration is increased can be seen from this graph. The packing density is seen to increase as the precursor concentration is increased which agrees with the results obtained by Zhang et. al[42] when they change the precursor concentration under similar conditions. As it was discussed earlier, the primary particle size of the titanium oxide nanoparticles is proportional to the TTIP concentration. The average primary particle size increases as the precursor concentration is increased[41,54,55]. When the TTIP concentration is low, the number of particles in the flame is less. Hence, the possibility of the particle aggregation in the flame to increase the diameter of the nuclei is less. As a result, the primary particle size incident on the film decreases and hence the film is less dense[42]. Inversely, when the precursor concentration increases, the number of particles in the flame increase and aggregate together to increase the size of their nuclei. Thus, particles have high primary particle size when they are incident on the film. This creates a more packed film and

increases the packing density. The packing density trend in figure 6.8 is similar by experiment and model calculations.

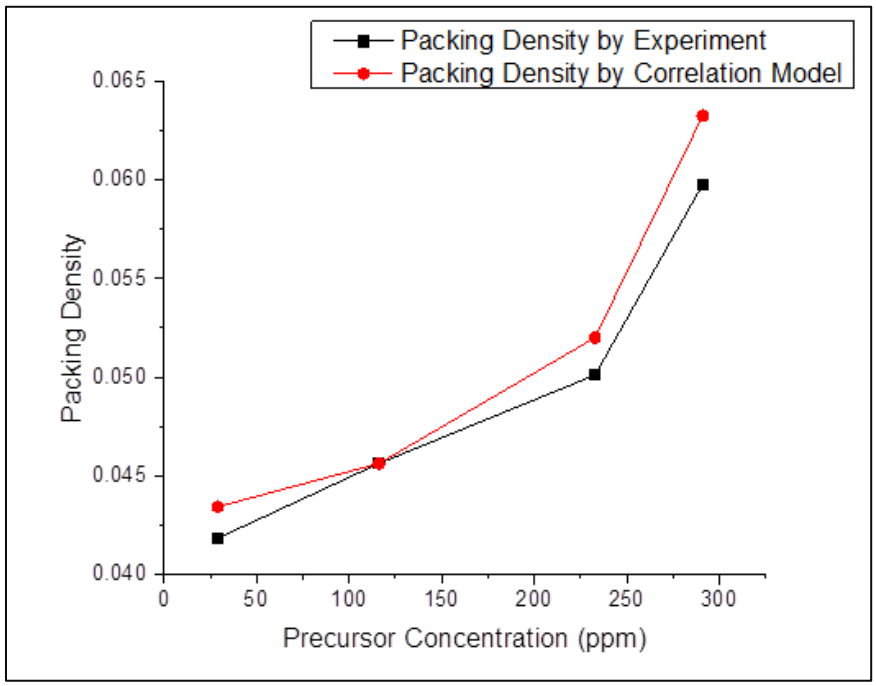

Figure 6.8. Graph of Packing Density versus Precursor Concentration at 29.1ppm, 116ppm, 232.8ppm, 291ppm and constant substrate temperature of 763 K.

CHAPTER 7

CONCLUSION AND FUTURE SCOPE

7.1 Conclusion

VOLTAGE	CASE 1	CASE 2	CASE 3	CASE 4	CASE 5	CASE 6
-800	31.91	44.84	54.26	44.34	55.99	25.74
-600	29.38	33.70	53.64	33.55	49.75	34.95
-400	51.29	41.71	70.15	22.05	46.98	34.35
-200	57.91	40.94	61.37	23.92	47.59	41.62
0	22.57	41.33	57.16	39.26	44.06	26.23
+200	48.46	38.10	56.75	13.70	47.29	30.94
+400	44.54	49.14	70.19	28.49	37.12	30.56
+600	27.70	46.02	54.80	20.07	33.20	25.58
+800	31.67	50.51	52.87	43.24	50.80	29.89

Table 7.1. Thickness of the TiO_2 films in μm for all the cases.

VOLTAGE	CASE 1	CASE 2	CASE 3	CASE 4	CASE 5	CASE 6
-800	Anatase	Anatase	Anatase	Anatase+Rutile	Anatase	Anatase
-600	Anatase	Anatase	Anatase	Anatase+Rutile	Anatase	Anatase
-400	Anatase	Anatase	Anatase	Anatase+Rutile	Anatase	Anatase
-200	Anatase	Anatase	Anatase	Anatase+Rutile	Anatase	Anatase
0	Anatase	Anatase	Anatase	Anatase+Rutile	Anatase	Anatase

+200	Anatase	Anatase	Anatase	Anatase+Rutile	Anatase	Anatase
+400	Anatase	Anatase	Anatase	Anatase+Rutile	Anatase	Anatase
+600	Anatase	Anatase	Anatase	Anatase+Rutile	Anatase	Anatase
+800	Anatase	Anatase	Anatase	Anatase+Rutile	Anatase	Anatase

Table 7.2. Phase of the particles in the TiO_2 films for all the cases.

- Particle deposition and structure on a film in a stagnation swirl flame is governed by the thermophoretic effect and Brownian motion, while the particle growth and aggregate size depends on the in-flame agglomeration when the substrate temperature is low and on the on-substrate sintering when the substrate temperature is high.

- When a voltage is applied to the substrate, the electrophoretic effect along with the Brownian motion and thermophoretic effect will govern the growth, structure and deposition of the titanium oxide nanoparticles in the film.

- For a given polarity of the voltage, the size of the particles decreases at lower voltages up to |±400 V| while it increases at higher voltages above |±400 V|. The average diameter of the primary particles is less under a negative voltage than that at a positive voltage.

- For a given substrate temperature and precursor concentration, the packing density of the TiO_2 film decreases at low voltages till |±400 V| after which it

increases at higher voltages up to |±800 V|. The packing density of the film is lowest at -400 V. The packing density of the films at lower voltages up to |±400 V| is lesser under the effect of a negative voltage than it is under the effect of a positive voltage.

- At a constant precursor concentration and in the absence of any applied voltage, the packing density of the TiO_2 film first decreases when the substrate temperature is increased from 473K to 663K and increases when the substrate temperature is further increased till 763K.

- At a constant substrate temperature and in the absence of any applied voltage, the packing density of the film increases as the precursor concentration is increased from 29.1 ppm to 291 ppm

- The applied voltage does not have any effect on the phase of the nanoparticles. The titanium oxide nanoparticles are anatase in phase, with the only exception being when the precursor concentration is very low at 29.1 ppm, with a long experimental duration; and the substrate temperature is 763 K. For this case, the titania nanopowders have a small rutile content along with the anatase.

7.2 Future Scope

In section 1.1, it was mentioned that titanium oxide nanostructured films are used in the application of dye sensitized solar cells to absorb the electrons due to the photo-excitation of the dye. The efficiency of the DSSCs depends on the diffusion of the electrons in the TiO_2 film, which in turn depends on the porosity of the films. In this work, we have studied how the applied voltage can affect the porosity of the films. In future work, the next step will be to test the efficiency of these films in the DSSCs. Performance tests on the DSSCs using TiO_2 films synthesized under different voltages will determine which case with the ideal substrate temperature, precursor concentration, and applied voltage gives the highest efficiency on the DSSCs. As seen from the results, the films have highest porosity at -400 V, for our setups. It will be interesting to see if the performance tests show the DSSCs have the highest efficiency when this film is used.

In-situ laser diagnostics methods can be used to further understand regimes that control the growth and structure of the nanoparticles in the film. Laser diagnostics techniques like Raman spectroscopy and laser induced breakdown spectroscopy (LIBS) can be used to determine if the applied voltage is affecting the flame structure and deposited particle characteristics. Another step will be to dope metals into the titanium oxide films to alter their properties.

References

1. Shi, H., Magaye, R., Castranova, V. & Zhao, J. Titanium dioxide nanoparticles: a review of current toxicological data. *Part Fibre Toxicol* **10,** 15 (2013).
2. Matijevic, E. Monodispersed colloids: art and science. *Langmuir* **2,** 12–20 (1986).
3. Sugimoto, T. Preparation of monodispersed colloidal particles. *Adv. Colloid Interface Sci.* **28,** 65–108 (1987).
4. Reyes-Coronado, D. *et al.* Phase-pure TiO2 nanoparticles: anatase, brookite and rutile. *Nanotechnology* **19,** 145605 (2008).
5. Sang, L., Zhao, Y. & Burda, C. TiO2 Nanoparticles as Functional Building Blocks. *Chem. Rev.* **114,** 9283–9318 (2014).
6. Gupta, S. M. & Tripathi, M. A review of TiO2 nanoparticles. *Chin. Sci. Bull.* **56,** 1639–1657 (2011).
7. Greenwood, N. N. & Earnshaw, A. *Chemistry of the elements*. (Pergamon Press, 1984).
8. Hatch, F. H. *Mineralogy*. (Whittaker & Company, 1912).
9. Warheit, D. B., Webb, T. R., Reed, K. L., Frerichs, S. & Sayes, C. M. Pulmonary toxicity study in rats with three forms of ultrafine-TiO2 particles: differential responses related to surface properties. *Toxicology* **230,** 90–104 (2007).
10. Sayes, C. M. *et al.* Correlating nanoscale titania structure with toxicity: a cytotoxicity and inflammatory response study with human dermal fibroblasts and human lung epithelial cells. *Toxicol. Sci. Off. J. Soc. Toxicol.* **92,** 174–185 (2006).
11. Zhang, H. & Banfield, J. F. Thermodynamic analysis of phase stability of nanocrystalline titania. *J. Mater. Chem.* **8,** 2073–2076 (1998).

12. Zhang, H. & Banfield, J. F. Understanding Polymorphic Phase Transformation Behavior during Growth of Nanocrystalline Aggregates: Insights from TiO2. *J. Phys. Chem. B* **104,** 3481–3487 (2000).

13. Navrotsky, A. Energetics of nanoparticle oxides: interplay between surface energy and polymorphism†. *Geochem. Trans.* **4,** 34 (2003).

14. Naicker, P. K., Cummings, P. T., Zhang, H. & Banfield, J. F. Characterization of Titanium Dioxide Nanoparticles Using Molecular Dynamics Simulations. *J. Phys. Chem. B* **109,** 15243–15249 (2005).

15. Anderson, M. A., Gieselmann, M. J. & Xu, Q. Titania and alumina ceramic membranes. *J. Membr. Sci.* **39,** 243–258 (1988).

16. Penn, R. L. & Banfield, J. F. Morphology development and crystal growth in nanocrystalline aggregates under hydrothermal conditions: insights from titania. *Geochim. Cosmochim. Acta* **63,** 1549–1557 (1999).

17. Barbé, C. J. *et al.* Nanocrystalline Titanium Oxide Electrodes for Photovoltaic Applications. *J. Am. Ceram. Soc.* **80,** 3157–3171 (1997).

18. Zaban, A., Aruna, S. T., Tirosh, S., Gregg, B. A. & Mastai, Y. The Effect of the Preparation Condition of TiO2 Colloids on Their Surface Structures. *J. Phys. Chem. B* **104,** 4130–4133 (2000).

19. Zhang, Z., Wang, C.-C., Zakaria, R. & Ying, J. Y. Role of Particle Size in Nanocrystalline TiO2-Based Photocatalysts. *J. Phys. Chem. B* **102,** 10871–10878 (1998).

20. Oskam, G., Nellore, A., Penn, R. L. & Searson, P. C. The Growth Kinetics of TiO2 Nanoparticles from Titanium(IV) Alkoxide at High Water/Titanium Ratio. *J. Phys. Chem. B* **107,** 1734–1738 (2003).

21. Weir, A., Westerhoff, P., Fabricius, L., Hristovski, K. & von Goetz, N. Titanium Dioxide Nanoparticles in Food and Personal Care Products. *Environ. Sci. Technol.* **46,** 2242–2250 (2012).

22. Wolf, R., Matz, H., Orion, E. & Lipozencić, J. Sunscreens--the ultimate cosmetic. *Acta Dermatovenerol. Croat. ADC* **11,** 158–162 (2003).

23. Kaida, T., Kobayashi, K., Adachi, M. & Suzuki, F. Optical characteristics of titanium oxide interference film and the film laminated with oxides and their applications for cosmetics. *J. Cosmet. Sci.* **55,** 219–220 (2004).

24. Kurtoglu, M. E., Longenbach, T. & Gogotsi, Y. Preventing Sodium Poisoning of Photocatalytic TiO2 Films on Glass by Metal Doping. *Int. J. Appl. Glass Sci.* **2,** 108–116 (2011).

25. Carp, O. Photoinduced reactivity of titanium dioxide. *Prog. Solid State Chem.* **32,** 33–177 (2004).

26. Fujishima, A. & Honda, K. Electrochemical Photolysis of Water at a Semiconductor Electrode. *Nature* **238,** 37–38 (1972).

27. Ochiai, T. & Fujishima, A. Photoelectrochemical properties of TiO2 photocatalyst and its applications for environmental purification. *J. Photochem. Photobiol. C Photochem. Rev.* **13,** 247–262 (2012).

28. Fujishima, A., Rao, T. N. & Tryk, D. A. Titanium dioxide photocatalysis. *J. Photochem. Photobiol. C Photochem. Rev.* **1,** 1–21 (2000).

29. Fujishima, A. & Zhang, X. Titanium dioxide photocatalysis: present situation and future approaches. *Comptes Rendus Chim.* **9,** 750–760 (2006).

30. Grätzel, M. Dye-sensitized solar cells. *J. Photochem. Photobiol. C Photochem. Rev.* **4,** 145–153 (2003).

31. Kambili, A. *et al.* Electron transport in the dye sensitized nanocrystalline cell. *Phys. E Low-Dimens. Syst. Nanostructures* **14,** 203–209 (2002).

32. Nakade, S. *et al.* Influence of TiO_2 Nanoparticle Size on Electron Diffusion and Recombination in Dye-Sensitized TiO_2 Solar Cells. *J. Phys. Chem. B* **107,** 8607–8611 (2003).

33. Nikraz, S., Phares, D. J. & Wang, H. Mesoporous titania films prepared by flame stabilized on a rotating surface: application in dye sensitized solar cells. *J. Phys. Chem. C* **116,** 5342–5351 (2012).

34. Lee, S. *et al.* Two-Step Sol−Gel Method-Based TiO2 Nanoparticles with Uniform Morphology and Size for Efficient Photo-Energy Conversion Devices. *Chem. Mater.* **22,** 1958–1965 (2010).

35. Sugimoto, T., Zhou, X. & Muramatsu, A. Synthesis of uniform anatase TiO2 nanoparticles by gel–sol method: 3. Formation process and size control. *J. Colloid Interface Sci.* **259,** 43–52 (2003).

36. Burnside, S. D. *et al.* Self-Organization of TiO2 Nanoparticles in Thin Films. *Chem. Mater.* **10,** 2419–2425 (1998).

37. Ehrman, S. H., Friedlander, S. K. & Zachariah, M. R. Characteristics of SiO< sub> 2</sub>/TiO< sub> 2</sub> nanocomposite particles formed in a premixed flat flame. *J. Aerosol Sci.* **29,** 687–706 (1998).

38. Kavitha, R., Meghani, S. & Jayaram, V. Synthesis of titania films by combustion flame spray pyrolysis technique and its characterization for photocatalysis. *Mater. Sci. Eng. B* **139,** 134–140 (2007).

39. Thimsen, E. & Biswas, P. Nanostructured photoactive films synthesized by a flame aerosol reactor. *AIChE J.* **53,** 1727–1735 (2007).

40. Zhao, H., Liu, X. & Tse, S. D. Effects of pressure and precursor loading in the flame synthesis of titania nanoparticles. *J. Aerosol Sci.* **40,** 919–937 (2009).

41. Wang, J., Li, S., Yan, W., Tse, S. D. & Yao, Q. Synthesis of TiO2 nanoparticles by premixed stagnation swirl flames. *Proc. Combust. Inst.* **33,** 1925–1932 (2011).

42. Zhang, Y., Shuiqing, L., Deng, S., Yao, Q. & Tse, S. D. Direct synthesis of nanostructured TiO< sub> 2</sub> films with controlled morphologies by stagnation swirl flames. *J. Aerosol Sci.* **44,** 71–82 (2012).

43. Macwan, D. P., Dave, P. N. & Chaturvedi, S. A review on nano-TiO2 sol–gel type syntheses and its applications. *J. Mater. Sci.* **46,** 3669–3686 (2011).

44. Kammler, H. K., Jossen, R., Morrison Jr, P. W., Pratsinis, S. E. & Beaucage, G. The effect of external electric fields during flame synthesis of titania. *Powder Technol.* **135,** 310–320 (2003).

45. Katzer, M., Weber, A. P. & Kasper, G. The effects of electrical fields on growth of titania particles formed in a CH< sub> 4</sub>–O< sub> 2</sub> diffusion flame. *J. Aerosol Sci.* **32,** 1045–1067 (2001).

46. Zhao, H., Liu, X. & Tse, S. D. Control of nanoparticle size and agglomeration through electric-field-enhanced flame synthesis. *J. Nanoparticle Res.* **10,** 907–923 (2008).

47. Einstein, A. Über die von der molekularkinetischen Theorie der Wärme geforderte Bewegung von in ruhenden Flüssigkeiten suspendierten Teilchen. *Ann. Phys.* **322,** 549–560 (1905).

48. Vincenti, W. G. & Krüger, C. H. *Introduction to Physical Gas Dynamics*. (John Wiley & Sons, 1965).

49. Friedlander, S. K. *Smoke, dust, and haze: fundamentals of aerosol dynamics*. (Oxford University Press, 2000).

50. S. K Friedlander, J. F. de la M. Diffusive leakage of small particles across the dust-free layer near a hot wall. *J. Colloid Interface Sci.* **125,** 351–355 (1988).

51. Hinds, W. C. *Aerosol technology: properties, behavior, and measurement of airborne particles*. (Wiley, 1999).

52. Kulkarni, P. & Biswas, P. A Brownian dynamics simulation to predict morphology of nanoparticle deposits in the presence of interparticle interactions. *Aerosol Sci. Technol.* **38,** 541–554 (2004).

53. Thimsen, E., Rastgar, N. & Biswas, P. Nanostructured TiO_2 Films with Controlled Morphology Synthesized in a Single Step Process: Performance of Dye-Sensitized Solar Cells and Photo Watersplitting. *J. Phys. Chem. C* **112,** 4134–4140 (2008).

54. Baron, P. A. & Willeke, K. *Aerosol measurement: principles, techniques, and applications*. (Wiley, 2001).

55. Pratsinis, S. E. Flame aerosol synthesis of ceramic powders. *Prog. Energy Combust. Sci.* **24,** 197–219 (1998).

56. Xing, Y., Köylü, Ü. Ö. & Rosner, D. E. Synthesis and restructuring of inorganic nano-particles in counterflow diffusion flames. *Combust. Flame* **107,** 85–102 (1996).